S. Afr. J. Chem., 2023, 77, 48–60
https://journals.co.za/content/journal/chem/

Mononuclear discrete Ag(I) complexes of aryl substituted (*E*)-*N*-phenyl-1-(pyridin-3-yl)methanimine: *In vitro* biological activities and interactions with biomolecules

Adesola A. Adeleke[1,2], Md. Shahidul Islam[3], Kolawole Olofinsan[3], Veronica F. Salau[3] and Bernard Omondi*[1]

[1]*School of Chemistry and Physics, University of KwaZulu-Natal, South Africa*
[2]*Department of Chemical Sciences, Olabisi OnabanJo University, Ago-Iwoye, Nigeria*
[3]*Discipline of Biochemistry, School of Life Sciences, University of KwaZulu-Natal, Durban, South Africa*

ABSTRACT

The synthesis of three pyridinyl imines (L1–L3) with electron-donating and electron-withdrawing functional groups, as well as their silver(I) complexes (1a–3a, 1b–3b and 1c–3c), resulted from our ongoing search for novel metallodrugs with potential pharmacological activity. Various analytical and spectroscopic analyses were used to characterize the Ag(I) complexes. The single crystal X-ray diffraction analysis of complexes 3a and 3b in the solid state confirmed their linear geometry around the Ag(I) center. *In vitro* antibacterial properties of the complexes evaluated using the minimum inhibitory concentration (MIC) method revealed that complexes containing either a Me- or an F-substituent exhibited greater activity. The ferric-reducing antioxidant power (FRAP) experiment revealed that complexes with hydroxyl substituents have high antioxidant potential. These complexes with IC_{50} values ranging from 0.86 to 2.47 mg mL^{-1} outperformed ascorbic acid, with an IC_{50} of 2.68 mg mL^{-1}. The reported complexes bound to CT-DNA *via* intercalation mode with significant binding constants for complexes whose ligands bore the OH^- substituent. Bovine serum albumin (BSA) binding affinity to the complexes ranges from moderate to high. The studied complexes with methyl substituents are promising anti-cervical cancer candidates.

KEYWORDS

3-pyridinyl Schiff bases, anion variation, anticancer, discrete Ag(I) complexes

Received 16 June 2022, revised 11 March 2023, accepted 23 March 2023

INTRODUCTION

Imine represents one of the most extensively used organic compounds in various chemistry areas such as synthetic chemistry,[1,2,3] catalysis,[4] electrochemistry,[5] materials science,[6] and pharmaceutical chemistry.[7,8,9] The main structural feature of an imine compound with general formula (R_1–CH = N–R_2) is the carbon-to-nitrogen double bond, where R represents a variable substituted alkyl or aryl group. The structure of Schiff bases is fundamental for their function in biological applications. Pyridinyl Schiff bases characterized by pyridinyl and a phenyl ring linked by an azomethine group have been of great interest because of their wide applications in various fields. It is known that free pyridinyl Schiff bases possess good biological activities, but when administrated as metal complexes, the bioactivity of the Schiff base is enhanced.[10] Transition metals have gained a significant position in medicine because of the significant progress in using metallodrugs to treat several human diseases. Recent studies showed that transition metal complexes are potential biological agents such as antitumor,[11] antiviral,[12] anti-diabetes,[13] antioxidant[14] and antimicrobial.[15] Among these transition metals, Ag(I) complexes have a promising future in medicine as therapeutic agents. This is related to Ag(I) complexes' exceptional chemical and biological features, such as variable chelating ability, high stability, high bio-activity at low concentrations, high selectivity and low toxicity to human beings.

Cancer is the world's second-largest cause of death. As a result, finding novel and more effective anticancer drugs with high cytotoxicity is critical. Over the years, various transition metal complexes as anticancer agents[11,16,17,18] have been reported, but their usage has either been stopped or limited due to severe side effects, such as high toxicity to human beings, nephrotoxicity, neurotoxicity, ototoxicity, as haemolytic anaemia, drug resistance, poor selectivity and low bioavailability. Among the commonly used transition metals as anticancer agents, the literature has described Ag(I) complexes as one of the leading antitumor agents owing to their effective cytotoxicity against various tumour cells.

The evaluation of transition metal complexes' interactions with biomolecules, including DNA and proteins, is noted to have a key role in developing therapeutic agents. Since DNA contains all cellular information, the study of DNA interaction with a potential therapeutic agent that targets DNA is crucial. For example, The majority of anticancer medicines target DNA. In cancer cells, interactions between DNA and small molecules can cause damage, impede cell division, and lead to cell death. Ag(I) complexes have been recognized as good DNA binders. They can bind with DNA via different modes such as intercalation, groove and external electrostatic interaction. Likewise, the binding affinity of Ag(I) complexes with serum albumins have been intensively studied. A potential drug should possess a binding affinity to a carrier protein in the blood to be delivered to the expected target cells. Serum albumin, being the most important carrier protein in the blood, can bind with drug molecules and form a stable protein-drug complex affecting the absorption, distribution, activity and toxicity of such drugs. [19]

Notably, in searching for new and effective antimicrobial agents to curtail the incessant resistance of microbes to antimicrobials, Ag(I) complexes have proven to be an alternative antimicrobial agent, as gathered from the literature.[20,21,22,23] In like manner, many Ag(I) complexes with antioxidant properties[24,25,26] have been developed. They can slow down or hinder the oxidation of biomolecules by terminating the free radicals' initiation or propagation reaction chains.

In continuation of our efforts in designing new Ag(I) complexes of pyridinyl Schiff bases as potential therapeutic agents, we report here the synthesis and characterization of pyridinyl functionalized Schiff bases obtained from the condensation reaction of 3-pyridinecarboxaldehyde with 2-aminophenol, 1-amino-*2*-fluorobenzene, and 4-methylaniline, respectively, and their Ag(I) complexes. The interaction of the pyridinyl Ag(I) complexes with DNA and Bovine serum albumin

*To whom correspondence should be addressed
Email: owaga@ukzn.ac.za

ISSN 1996-840X Online / South African Chemical Institute / http://saci.co.za/journal
© The Author(s) Published under a Creative Commons Attribution 4.0 International Licence (CC BY 4.0)
https://doi.org/10.17159/0379-4350/2023/v77a08

(BSA) and their antioxidant, antibacterial, and cytotoxicity assay were investigated.

EXPERIMENTAL

Materials and Methods

Local suppliers provided 3-pyridinecarboxaldehyde 99% (Aldrich, USA), 2-aminophenol >99% (Aldrich, USA), 4-methylaniline 99.5% (Aldrich, USA), 1-amino-2-fluorobenzene 99.5% (Aldrich, USA), calf-thymus DNA (CT-DNA), ethidium bromide 95% (Aldrich, USA), bovine serum albumin 99% (Aldrich, USA), >99% ethanol (Aldrich, USA), >99% diethyl ether (Aldrich, USA) and >99% DMSO-*d6* (Merck, Germany). All of the chemicals were of analytical quality and were utilized as received, with the exception of the solvents, which were dried using traditional methods.

On a BRUKER 400 MHz spectrometer, ^{1}H and ^{13}C NMR spectra in DMSO-*d6* and acetone-*d6* were obtained. Chemical shift values in DMSO-*d6* and acetone-*d6* are presented in parts per million (ppm) relative to the solvent residual peaks; 2.5 and 2.05 ppm for ^{1}H NMR and 39.5 and 29.4 ppm for ^{13}C NMR, respectively. S stands for singlet, d for doublet, and m for multiplet in the splitting patterns of ^{1}H NMR spectra, whereas J (in hertz) stands for the coupling constant. The infrared spectra were captured with an Agilent Cary 630 spectrometer, and the results are presented as percentage transmittances at various wavenumbers (cm^{-1}), ranging from 4000 to 650 cm^{-1}. Only molecular ions (M+) and significant fragmentation peaks were reported in the mass spectra, with intensities expressed as percentages of the base peak, using a Shimadzu LCMS-2020 instrument. Thermal-Scientific Flash 2000 CHNS/O analyzer was used to conduct elemental studies. The Stuart Scientific melting point device was used to determine all melting points. The Shimadzu UV-1800 UV-Vis Spectrophotometer was used to measure the absorption of CT-DNA and protein. A PerkinElmer LS 45 Fluorescence Spectrometer was used to record photoluminescence investigations of CT-DNA and protein.

Synthesis of pyridinyl Schiff bases L1–L3

Schiff bases (*E*)-2-((pyridin-3-ylmethylene)amino)phenol (**L1**), (*E*)-*N*-(2-fluorophenyl)-1-(pyridin-3-yl)methanimine (**L2**) and (*E*)-1-(pyridin-3-yl)-*N*-(p-tolyl)methanimine (**L3**) were synthesized using a slightly modified literature procedures.[3,27,28] In the presence of glacial acetic acid, a hot solution of 3-pyridinecarboxaldehyde (1 mmol,~0.1 mL) in anhydrous ethanol (10 mL) was added to a hot solution of 2-aminophenol (1 mmol, 0.1 g), 1-amino-2-fluorobenzene (1 mmol, 0.1 mL), and 4-methylaniline (1 mmol, 0.11 g) respectively. The resultant reaction was refluxed at 80 °C for 4 h. Under reduced pressure, **L1** and **L3** solutions were evaporated to one-third of their original volume, and ether (10 mL) was added to each solution to produce a precipitate. Filtration was used to extract the precipitates, then rinsed with cold ether (10 mL ×2) and recrystallized from ethanol. The **L2** solution, on the other hand, was entirely evaporated under pressure, with the resulting oil being recrystallized from ethanol.

Synthesis of Ag(I) complexes of pyridinyl Schiff bases (1a–3a, 1b–3b and 1c–3c)

Nine Ag(I) complexes numbered **1a–3a**, **1b–3b** and **1c–3c** were synthesized following our reported procedures.[29] Under constant stirring in the dark, complexes **1a–3a**, **1b–3b** and **1c–3c** were synthesized by dropwise addition of ethanol solution of each of **L1–L3** (1 mmol) to an ethanol solution of $AgNO_3$ (0.5 mmol, 0.10g), $AgClO_4$ (0.5 mmol, ~0.10 g), and $AgCF_3SO_3$ (0.5 mmol, 0.13 g). For 6 hours, the reaction was carried out under N_2 gas at room temperature. Vacuum filtering was later used to separate the precipitates that resulted. The precipitates were washed twice with cold ethanol, then twice with cold ether, before being dried in a vacuum. The isolated Ag(I) complexes were recrystallized by dissolving the complexes in dichloromethane and layering them with toluene.

[Ag(L1)$_2$]NO$_3$ 1a

Colour: green, yield: 0.18 g, 64%, m.p 141–142 °C. ^{1}H-NMR (400 MHz, DMSO-*d6*, 25 °C): δ ppm = 9.14 (1H, s, Hj-OH), 9.05 (1H, s, Hd-pyr), 8.80 (1H, s, He-C=N-), 8.69 (1H, s, Hc-pyr), 8.45 (1H, d, J = 7.82 Hz, Ha-pyr), 7.55 (1H, q, J = 4.74 Hz, Hb-pyr), 7.26 (1H, t, J = 7.88 Hz, Hf-ary), 7.11 (1H, m, Hi-ary), 6.92 (1H, d, J = 8.16 Hz, Hh-ary), 6.85 (1H, q, J = 7.57 Hz, Hg-ary). ^{13}C-NMR (100 MHz, DMSO-*d6*, 25 °C): δ = 156.76 (C6- C=N-), 154.62 (C3-pyr), 151.45(C12-ary), 150.30 (C4-pyr), 137.35 (C7-ary), 136.16 (C1-pyr), 135.70 (C5-pyr), 128.05 (C10-ary), 119.59 (C2- pyr), 119.14 (C9-ary), 116.23 (C11-ary), 115.77 (C8-ary). FT-IR (cm^{-1}): 3336, 3038, 1624, 1576. UV/Vis (acetonitrile): λ_{max} 290, 347, 357 nm. MS: *m/z* Calcd. For [$C_{24}H_{20}AgN_4O_2$]: 504.32; found [Ag(L1)$_2$+MeOH+K]$^+$ 575 (11%), [Ag(L1-OH)]$^+$ 288 (100%). Anal. Calcd. (%) for ($C_{24}H_{20}AgN_5O_5$): C, 50.90; H, 3.56; N, 12.37; found (%): C, 50.81; H, 3.42; N, 12.36.

[Ag(L2)$_2$]NO$_3$ 2a

Colour: brown, yield: 0.25 g, 86%, m.p 171–172 °C. ^{1}H-NMR (400 MHz, DMSO-*d6*, δ ppm): 9.09 (2H, d, Hd-pyr), 8.78 (2H, s, He-CH=N), 8.74 (2H, m, Hc- pyr), 8.38 (2H, Ha- pyr), 7.62 (2H, m, Hb-pyr), 7.31 (8H, m, Hf, g, h, i-ary). ^{13}C-NMR (100 MHz, DMSO-*d6*, 25 °C): δ = 160.89 (C6- C=N-), 154.66 (C12- ary), 152.47 (C3- pyr), 150.66 (C4- pyr), 136.32 (C7- ary), 135.71 (C1- pyr), 131.50 (C5-pyr), 127.74 (C10- ary), 125.02 (C9- ary), 124.49 (C2- pyr), 124.36 (C8- ary). 116.26 (C11- ary). FT-IR (cm^{-1}): (Ar-CH) 3254, (-C=N-) 1625, (pyridinyl) 1590, (C-F) 1488. UV/Vis (acetonitrile): λ_{max} 235, 323 nm. MS: *m/z* Calcd. For [$C_{24}H_{18}AgF_2N_4$]: 508.30; found [Ag(L3) + H]$^+$: 509 (100%), [AgL + Na+CH_3CN + 2EtOH] $^+$: 463 (67%), [AgL + CH_3CN+H]$^+$: 350 (20%). Anal. Calcd. (%) for ($C_{24}H_{18}AgF_2N_5O_3$): C, 50.55; H, 3.18; N, 12.28; found (%): C, 50.39; H, 3.11; N, 12.10.

[Ag(L3)$_2$]NO$_3$ 3a

Colour: white, yield: 0.26 g, 93%, m.p 159–160 °C. ^{1}H-NMR (400 MHz, DMSO-*d6*, δ ppm): 9.07 (1H, s, Hd-pyr), 8.69 (2H, t, J = 1.72 Hz, 1.72 Hz, He-CH=N-, Hc-pyr), 8.32 (1H, m, Ha-pyr), 7.49 (1H, m, Hb-pyr), 7.23 (4H, s, Hf-ary), 2.36 (3H, s, Hg-CH_3). ^{13}C-NMR (100 MHz, DMSO-*d6*, 25 °C): δ = 157.33 (C6- C=N-), 151.91 (C3- pyr), 150.40 (C4- pyr), 148.29 (C7- ary), 135.94 (C10- ary), 135.23 (C1- pyr), 131.81 (C5- pyr), 129.71 (C9- ary , C12- ary), 124.19 (C2- pyr), 121.04 (C8- ary, C13- ary), 20.55 (C11- CH_3). FT-IR (cm^{-1}): (Ar-CH) 3054, (-C=N-) 1622, (pyridinyl) 1595, (C-CH_3) 2895. UV/Vis (acetonitrile): λ_{max} 287, 324 nm. MS: *m/z* Calcd. For [$C_{26}H_{24}AgN_4$]: 500,37; found [Ag(L4)$_2$ + H]: 501 (68%), [Ag(L4)] + MeOH + Na]: 359 (100%); [Ag(L4) + MeOH]: 336 (88%). Anal. Calcd. (%) for ($C_{26}H_{24}AgN_5O_3$): C, 55.53; H, 4.30; N, 12.45; found (%): C, 55.52; H, 4.27; N, 12.24.

[Ag(L1)$_2$]ClO$_4$ 1b

Colour: brown, yield: 0.25 g, 83%, m.p 174–175 °C. ^{1}H-NMR (400 MHz, DMSO-*d6*, 25 °C): δ ppm = 9.16 (2H, d, Hi-OH), 9.07 (2H, s, Hd-pyr), 8.83 (2H, s, H-C=N-), 8.70 (2H, q, J = 4.78 Hz, Hc-pyr), 8.47 (2H, d, J = 7.93 Hz, Ha-pyr), 7.57 (2H, q, J = 4.64 Hz, Hb-pyr), 7.28 (2H, q, J = 7.86 Hz, Hf- ary), 7.13 (2H, m, Hh-ary), 6.90 (4H, m, Hg- ary). ^{13}C-NMR (100 MHz, DMSO-*d6*, 25 °C): δ = 157.24 (C6-C=N-), 155.07 (C3- pyr), 151.91 (C12- ary), 150.88 (C4- pyr), 137.81 (C7- ary), 136.57 (C1- pyr), 135.97 (C5- pyr), 128.45 (C10- ary), 120.01 (C2- pyr), 119.97 (C9- ary), 119.57 (C11- ary), 116.66 (C8- ary). FT-IR(cm^{-1}); 3393, 1625, 1582, 1481, 1147, 1069. UV/Vis (acetonitrile): λ_{max} 290, 348, 356 nm. MS *m/z*: Calcd. for [Ag(L1)$_2$]: 504.32; found [Ag(L1)$_2$+Na+2H] 529 (78%); [Ag(L1)$_2$+2EtOH+CH_3CN] 636 (34%); [Ag(L1)$_2$+EtOH+H] 551 (17%). Anal. Calcd. (%) for [Ag(L1)$_2$]ClO_4. C, 47.74; H, 3.34; N, 9.28; found (%): C, 47.55; H, 3.28; N, 9.03.

[Ag(L2)$_2$]ClO$_4$ 2b

Colour: white, yield: 0.23, 77%, m.p 250–251 °C, ^{1}H-NMR (400 MHz, DMSO-*d6*, δ ppm): 9.09 (2H, s, Hd-pyr), 8.78 (2H, s, He-CH=N), 8.74 (2H, m, Hc- pyr), 8.37 (2H, m, Ha- pyr), 7.62 (2H, m, Hb- pyr), 7.31 (8H, m, Hf, g, h, i-ary). ^{13}C-NMR (100 MHz, DMSO-*d6*, 25 °C): δ = 160.92 (C6- C=N-), 154.68 (C12- ary), 152.53 (C3- pyr), 150.71 (C4- pyr), 139.03 (C7- ary), 135.68 (C1- pyr), 131.50 (C5- pyr), 127.75 (C10- ary), 127.75 (C9- ary), 124.36 (C2- pyr, C8- ary). 116.07 (C11- ary). FT-IR (cm^{-1}): (Ar-CH) 3070, (-C=N-) 1621, (pyridyl) 1591, (C-F) 1490. UV/Vis (acetonitrile): λ_{max} 235, 323 nm. MS: *m/z* Calcd. For [$C_{24}H_{18}AgF_2N_4$]: 508.30; found [Ag(L3)$_2$ + H]$^+$: 509 (97%), [Ag(L3)$_2$ + CH_3CN + H]$^+$: 350 (21%). Anal. Calcd. (%) for ($C_{24}H_{18}AgClF_2N_4O_4$): C, 47.43; H, 2.99; N, 9.22; found (%): C, 47.41; H, 2.86; N, 9.28.

[Ag(L3)$_2$]ClO$_4$ 3b

Colour: white, yield: 0.29 g, 97%, m.p 205–206 °C. ^{1}H-NMR (400 MHz, DMSO-*d6*, δ ppm): 9.06 (2H, d, J = 1.60 Hz, Hd-pyr), 8.70 (4H, m, He-CH=N-, Hc-pyr), 8.32 (2H, m, Ha-pyr), 7.57 (2H, m, Hb-pyr), 7.24 (8H, s, Hf-ary), 2.33 (6H, s, Hg-CH_3). ^{13}C-NMR (100 MHz, DMSO-*d6*, 25 °C): δ = 157.68 (C6- C=N-), 152.21 (C3- pyr), 150.70 (C4- pyr), 148.63(C7- ary), 136.26 (C10- ary), 135.48 (C1- pyr), 132.09 (C5- pyr), 130.03 (C9- ary , C12- ary), 124.47 (C2- pyr), 121.36 (C8- ary, C13- ary), 20.88 (C11- CH_3). FT-IR (cm^{-1}): (Ar-CH) 3074, (-C=N-) 1624, (pyridinyl) 1597, (C-CH_3) 2908. UV/Vis (acetonitrile): λ_{max} 289, 324 nm. MS: *m/z* Calcd. For [$C_{26}H_{24}AgN_4$]: 500,37; found [Ag(L4)$_2$ + H]: 501 (100%). Anal. Calcd. (%) for ($C_{26}H_{24}AgClN_4O_4$): C, 52.06; H, 4.03; N, 9.34; found (%): C, 52.00; H, 4.16; N, 9.27.

[Ag(L1)$_2$]CF$_3$SO$_3$ 1c

Colour: brown, yield: 0.24 g, 73%, Decomp.: 184–185 °C. ^{1}H-NMR (400 MHz, DMSO-*d6*, 25 °C): δ ppm = 9.15 (2H, d, J = 1.67 Hz, Hj-OH), 9.08 (2H, d, J = 1.41 Hz, Hd-pyr), 8.81 (2H, s, He-CH=N-), 8.69 (2H, m, Hc-pyr), 8.47 (2H, m, Ha-pyr), 7.57 (2H, m, Hb-pyr), 7.26 (2H, m, Hf- ary), 7.12 (2H, m, Hh-ary), 6.88 (4H, m, Hg, i- ary). ^{13}C-NMR (100 MHz, DMSO-*d6*, 25 °C): δ = 156.66 (C6- C=N-), 154.57 (C3- pyr), 151.41 (C12- ary), 150.27 (C4- pyr), 137.28 (C7- ary), 136.13 (C1- pyr), 135.71 (C5- pyr), 128.00 (C10- ary), 124.41 (C2- pyr), 124.05 (C9- ary), 119.47 (C11- ary), 116.18 (C8- ary). FT-IR(cm^{-1}); 3396, 1627, 1582, 1483, 1147. UV/Vis (acetonitrile): λ_{max} 290, 348, 359 nm. MS *m/z*: Calcd. for [Ag(L1)$_2$]: 503.06 found [Ag(L-OH)$_2$ +2CH_3CN+Na] 575 (36%), [Ag(L1)$_2$+2EtOH+Na] 619 (15%); [Ag(L1)$_2$+CH_3CN] 545 (16%). Anal. Calcd. (%) for ($C_{25}H_{20}AgF_3N_4O_5S$): C, 45.96; H, 3.09; N, 8.58; found (%): C, 45.83; H, 3.05; N, 8.56.

[Ag(L2)$_2$]CF$_3$SO$_3$ 2c

Colour: white, yield: 0.28 g, 85%, Decomp.: 215–216 °C. ^{1}H-NMR (400 MHz, DMSO-*d6*, δ ppm): 9.10 (2H, d, J = 1.80 Hz, Hd-pyr), 8.80 (2H, s, He-CH=N), 8.76 (2H, m, Hc- pyr), 8.38 (2H, Ha- pyr), 7.63 (2H, m, Hb- pyr), 7.33 (8H, m, Hf, g, h, i-ary). ^{13}C-NMR (100 MHz, DMSO-*d6*, 25 °C): δ = 160.93 (C6- C=N-), 153.67 (C12- ary), 152.48 (C3- pyr), 150.68 (C4- pyr), 138.94 (C7- ary), 135.55 (C1- pyr), 131.45 (C5- pyr), 127.71 (C10- ary), 124.98 (C9- ary), 124.29 (C2- pyr), 121.40 (C2- pyr, C8- ary). 116.25 (C11- ary). FT-IR (cm^{-1}): (Ar-CH) 3064, (-C=N-) 1623, (pyridyl) 1592, (C-F) 1495. UV/Vis (acetonitrile): λ_{max} 235, 323 nm. MS: *m/z* Calcd. For [$C_{24}H_{18}AgF_2N_4$]: 508.30; found [Ag(L3)$_2$ + H]$^+$: 509 (25%), [Ag(L) + H]$^+$: 290 (100%). Anal. Calcd. (%) for ($C_{25}H_{18}AgF_5N_4O_3S$): C, 45.68; H, 2.76; N, 8.52; found (%): C, 45.65; H, 2.76; N, 8.42.

[Ag(L3)$_2$] CF$_3$SO$_3$ 3c

Colour: white, yield: 0.30 g, 91%, m.p 246–247 °C. ^{1}H-NMR (400 MHz, DMSO-*d6*, δ ppm): 9.07 (2H, d, J = 1.62 Hz, Hd-pyr), 8.71 (4H, t, He-CH=N-, Hc-pyr), 8.35 (2H, m, Ha-pyr), 7.61 (2H, m, Hb-pyr), 7.24 (8H, s, Hf-ary), 2.30 (6H, s, Hg-CH_3). ^{13}C-NMR (100 MHz, DMSO-*d6*, 25 °C): δ = 157.24 (C6- C=N-), 152.06 (C3- pyr), 150.50 (C4- pyr), 148.24 (C7- ary), 136.01 (C10- ary), 135.59 (C1- pyr), 131.94 (C5- pyr), 129.71 (C9- ary, C12- ary), 124.35 (C2- pyr), 121.06 (C8- ary, C13- ary), 20.55 (C11- CH_3). FT-IR (cm^{-1}): (Ar-CH) 3051, (-C=N-) 1625, (pyridyl) 1599, (C-CH_3) 2927. UV/Vis (acetonitrile): λ_{max} 291, 325 nm. MS: *m/z* Calcd. For [$C_{26}H_{24}AgN_4$]: 500,37; found [Ag(L4)$_2$ +L4+4]: 701 (42%), [Ag(L4)] + MeOH + Na]: 359 (100%); [Ag(L4) + 3MeOH]: 400 (26%). Anal. Calcd. (%) for ($C_{27}H_{24}AgF_3N_4O_3S$): C, 49.94; H, 3.73; N, 8.63; found (%): C, 49.94; H, 3.64; N, 8.68.

Single-crystal X-ray diffraction

On a Bruker Apex Duo diffractometer equipped with an Oxford Instruments Cryojet running at 100(2) K and an Incoatec microsource working at 30 W power, crystal evaluation and data gathering of [Ag(L3)$_2$]NO_3 (**3a**) and [Ag(L3)$_2$]ClO_4 (**3b**) were recorded. The results were collected using omega and phi scans with Mo K (= 0.71073) radiation at a crystal-to-detector distance of 50 mm. Outlier rejection, scan speed scaling, and standard Lorentz and polarization correction factors were used to reduce the data using the SAINT[30] programme. The data were subjected to a SADABS[31] semi-empirical multi-scan absorption adjustment.

The direct technique was used to solve and refine structures of **3a** and **3b** using the SHELXS[32] program. ORTEP-3[33] system software was used to visualize the crystal structure information. Non-hydrogen atoms were refined isotropically initially, then anisotropically using SHELXL[34] and a full-matrix least-squares approach based on F^2. During refinement, a non-crystallographic inversion center was detected in the crystal lattice of **3a**, and it was first suspected that the space group is centrosymmetric (C_2/c), but the solution had much worse refinement statistics. Thus, an inversion twin was modelled and refined with a BASF value of 0.6(1). All hydrogen atoms were geometrically positioned, permitted to ride on their parent atoms, and isotropically purified. Table 1 lists the crystallographic data and structure refinement parameters for **3a** and **3b**.

In vitro antimicrobial studies

The sterile nutrient agar medium was made as described by Njogu et al. 2017[35] by dissolving 38 g of MHA in distilled water (1 L). The resulting nutrient agar medium was sterilized by autoclaving for 15 minutes at 121°C and cooled in a water bath to 45°C. The cooled agar media was put onto Petri dishes with a uniform 4 mm depth and then cooled to room temperature. Ag(I) complexes **1a–3a**, **1b–3b**, **1c–3c**, as well as their ligands, were tested against six bacteria, including *Salmonella typhimurium* ATCC 14026, *Pseudomonas aeruginosa* ATCC 27853, *Escherichia coli* ATCC 25922, *Klebsiella pneumoniae* ATCC 31488, *Staphylococcus aureus* ATCC 700699 (methicillin-resistant) and *Staphylococcus aureus* ATCC 25923. The nutrient broth was prepared by dissolving 1.3 g in 100 mL of distilled water and sterilized at 121 °C. Approximately 10 mL of the sterile nutritional broth was transferred to cotton wool-plugged test tubes and coated with aluminum foil. The nutritional broth in the test tubes was autoclaved for 15 minutes at 121 °C before being cooled to 37 °C. Following that, a single colony of the bacteria was isolated and put into a 10 mL sterile NB, which was then cultured at 37 °C for 18 hours in a shaking incubator. Each bacteria strain concentration was adjusted with sterile distilled water to a final concentration of 1.5 × 10^8 cfu mL^{-1}. The antibacterial activity of **L1–L3** and **1a–3a**, **1b–3b** and **1c–3c** was first screened by spotting 5 µL of each concentration of **L1–L3** and **1a–3a**, **1b–3b** and **1c–3c** on an MHA petri dish and incubating at 37 °C for 18 hours. By looking for a clear zone at the spotting site, the antibacterial activity was calculated. The minimum inhibitory concentration (MIC) of the active compounds with putative antibacterial activities was determined against six bacteria. Ten serial dilutions of **L1–L3** and **1a–3a**, **1b–3b**, **1c–3c** were performed, and the solution was further

Table 1: Crystal data and structural refinement of $[Ag(L3)_2]NO_3$ (**3a**) and $[Ag(L3)_2]ClO_4$ (**3b**) complexes

	3a	**3b**
Chemical formula	$C_{130}H_{120}Ag_5N_{25}O_{15}$	$C_{13}H_{12}Ag_{0.5}Cl_{0.5}N_2O_2$
Formula weight	2811.87	299.91
Crystal system	Monoclinic	Monoclinic
Space group	Cc	C2/c
a(Å)	32.096(3)	28.190(3)
b(Å)	26.972(2)	5.4525(5)
c(Å)	13.8884(14)	16.2136(16)
α(°)	90	90
β(°)	101.550(5)	98.361(5)
γ(°)	90	90
V(Å^3)	11779.6(19)	2465.7(4)
Z	4	8
ρ_{calc}(gcm^{-3})	1.586	1.616
μ (mm^{-1})	0.895	0.967
F(000)	5720.0	1216.0
Crystal size (mm^3)	0.22 × 0.12 × 0.08	0.26 × 0.22 × 0.18
θ range for data collection (°)	2.59 to 55.754	2.92 to 53.38
Index ranges	−42 ≤ h ≤ 42 −35 ≤ k ≤ 35 −18 ≤ l ≤ 10	−35 ≤ h ≤ 35 −6 ≤ k ≤ 6 −20 ≤ l ≤ 20
Reflections collected	103404	19777
Independent reflections	21682 [R_{int} = 0.0460, R_{sigma} = 0.0427]	2597 [R_{int} = 0.0244, R_{sigma} = 0.0146]
Completeness to theta = 28.96	98.0%	99.6%
Data/restraints/parameters	21682/1058/1407	2597/0/166
Goodness-of-fit on F^2	1.124	1.123
R indices [I>2sigma(I)]	R_1 = 0.0509, wR_2 = 0.1167	R_1 = 0.0317, wR_2 = 0.1194
R indices (all data)	R_1 = 0.1001, wR_2 = 0.1492	R_1 = 0.0352, wR_2 = 0.1270
Largest diff. peak and hole (e Å^{-3})	1.81/−1.35	1.36/−0.84

diluted 5 times where the compounds had lower MICs. The MIC of the compounds was measured by spotting 5 μL of each concentration of **L1–L3** and **1a–3a**, **1b–3b**, **1c–3c** on MHA plates and incubating them at 37 °C for 18 hours. These procedures were carried out three times to determine the exact lowest concentration of the complexes at which no observable bacterial growth could be detected following incubation. As a reference, Ciprofloxacin was employed, while 0.5% DMSO was used as a negative control.[36]

Antioxidant assay

The ferric reducing capacity of **L1–L3** and **1a–3a**, **1b–3b** and **1c–3c** was measured using Benzie and Strain method[37] with slight modifications. Different concentrations ranging from 0.25 mg mL^{-1} to 2 mg mL^{-1} of **L1–L3** and **1a–3a**, **1b–3b** and **1c–3c**, as well as a standard (Ascorbic acid), were combined with 2.5 mL phosphate buffer (0.2 M) and 2.5 mL (1 percent w/v) potassium ferricyanide $[K_3Fe(CN)_6]$. The reaction mixture was acidified with 2.5 mL of trichloroacetic acid after 20 minutes of incubation at 50 °C (10%). After that, 1 mL of the acidified mixture was mixed with 1 mL of distilled water and 0.5 mL of iron (III) chloride (0.1%). The mixture's absorbance was then measured at 700 nm. Increased ferric reducing antioxidant power was shown by a decrease in absorbance. As shown in equation 1, the antioxidant power of the compounds can be expressed as a percentage of ferric reducing antioxidant power ascorbic acid equivalent.

$$\%\ \text{FRAP} = \frac{\text{absorbance of sample}}{\text{absorbance of ascorbic acid}} \times 100 \quad (1)$$

Cytotoxicity evaluation

The cytotoxicity of selected complexes; $[Ag(L3)_2]NO_3$ **(3a)**, $[Ag(L3)_2]ClO_4$ (**3b**), $[Ag(L3)_2]CF_3SO_3$ (**3c**) and Cisplatin as reference was evaluated on four human cell lines, human embryonic kidney 293 (HEK293), cervical cancer cell line (HELA), breast cancer cell line (MDA-MB231) and malignant human melanoma cell line (A375). Complexes **3a**, **3b** and **3c** were selected for cytotoxicity based on our previous study[38], where remarkable anticancer activity and high selectivity of Ag(I) complexes bearing the CH_3 substituent were identified. The cytotoxicity experiment was performed using Abrahams et al. 2018[39] methods, in which 1 × 10^5 cells per mL of HEK293 (non-cancerous cell line), HELA, MDA-MB231 and A375 were seeded in 96-well microtiter plates and allowed to stabilize for 4 hours at 37 °C and 5% CO_2. Then, through two-fold serial dilution, **3a**, **3b**, **3c** and Cisplatin were added to the plate, resulting in eight final compound concentrations ranging from 100 to 0.781 μM in a total volume of 200 μL per well. The plate was then incubated for 72 h at 37 °C and 5% CO_2. To each well, 20 μL CellTiter 96 AQ_{ueous} One Solution (Promega, Madison, WI, USA) was added, and the plates were incubated for 4 h as previously described. After that, absorbance was measured using a multiplate reader at 490 nm (Molecular Devices, San Jose, CA, USA). EC_{50} values were obtained using GraphPad Prism 8 (2019) (GraphPad Software, San Diego, CA, USA) to estimate the concentration of each complex required to lower cell viability by 50%. The values are averages of at least three experiments (n = 3).

DNA binding assay

As described in the literature[40,41] but with a slight modification, the calf thymus-DNA (CT-DNA) binding with **L1–L3** and complexes **1a–3a**, **1b–3b** and **1c–3c** was investigated using the absorption spectroscopy and fluorescence competitive displacement studies. The CT-DNA sodium salt was dissolved in phosphate buffer saline solution (PBS) pH 7.2 with continuous stirring overnight to make the DNA stock solution, filtered and kept at 4°C. UV-visible absorption with the absorption coefficient ε260 = 6600 M^{-1}cm^{-1} was used to calculate the final concentration of the CT-DNA. The CT-DNA has a 1.93 ratio at 260 and 280 nm UV absorbance, showing it is clean and devoid of protein contamination. A constant concentration (50 μM) of the complexes in DMSO was also prepared. The DNA titration assay was carried out by titrating between 0 and 30 μM of CT-DNA in PBS against constant concentrations (50 μM) of **L1–L3** and **1a–3a**, **1b–3b** and **1c–3c**. The compounds-CT-DNA mixture was incubated for 10 mins before the absorbance was measured using Shimadzu UV-1800 UV-Vis Spectrophotometer. An equal amount of CT-DNA was added to the reference solution to eliminate CT-DNA absorbance.

The Wolfe-Shimer equation (Equation 2) was used to get the intrinsic binding constant, K_b, of the compounds:

$$\frac{[DNA]}{\varepsilon_a - \varepsilon_f} = \frac{[DNA]}{\varepsilon_b - \varepsilon_f} + \frac{1}{K_b}(\varepsilon_b - \varepsilon_f) \quad (2)$$

where [DNA], ε_a, ε_b, and ε_f represent DNA concentration, apparent, fully bound complex, and free complex extinction coefficients, respectively. The binding constant K_b of the compounds was calculated as the ratio of the slope to the intercept from the plot of $[DNA]/(\varepsilon_a - \varepsilon_f)$ against [DNA].

Fluorescence competitive displacement study

In this study, a slightly modified method[42] was used for the competitive fluorescence displacement assay. In a phosphate buffer of pH 7.2, a

pre-treated 15 μM solution of ethidium bromide (EB) with 15 μM of CT-DNA was prepared and permitted to equilibrate for 30 mins. After that, different concentrations of the complexes (0–20 μM) were introduced at approximately 8 mins intervals for equilibration at room temperature, keeping CT-DNA-EB concentrations constant. The complexes' capacity to quench the fluorescence of CT-DNA bound EB was measured using a PerkinElmer LS 45 Fluorescence Spectrometer in the wavelength range of 530–700 nm at 25 °C with an excitation wavelength of 525 nm. The CT-DNA-EB fluorescence quenching of the complexes was evaluated using the Stern-Volmer Equation 3.

$$\frac{F_0}{F} = 1 + K_{SV}[Q] = 1 + K_q\tau_0[Q] \quad (3)$$

where F_0 and F denote the relative fluorescence intensities of CT-DNA in the absence and presence of the quencher, K_{sv} denotes the Stern-Volmer quenching constant, [Q], quencher concentration, K_q denotes the bimolecular quenching constant, and τ_0 denotes the average lifetime of the fluorophore in the absence of the quencher, which in biomacromolecules is typically equal to 10^{-8} s.

Albumin binding assay using absorption spectroscopy and fluorescence quenching method

Bovine serum albumin (BSA) stock solution was made by dissolving an adequate amount of BSA in phosphate buffer saline solution (pH 7.2) at 25 °C. The BSA concentration was measured spectrophotometrically using ε280 = 44300 $M^{-1}cm^{-1}$ absorption coefficient. The complex stock solution was made by dissolving 1 mmol of the complexes in DMSO. The absorption titration experiment was performed by adding various concentrations of the complexes (0–10 μM) to a constant BSA solution (6 μM). After adding the concentration, the sample solution was incubated for 10 mins at 25 °C before recording the absorbance at λ_{max} 280 nm. The intercept-to-slope ratio of 1/[A – A°] vs 1/[complex] linear curve was used to compute the binding constant K_b where A and A° denote BSA absorbance in the presence and absence of complexes, respectively.[43,44]

For the fluorescence quenching assay, a 1 μM BSA solution was titrated against various concentrations of the complexes (0–35 μM) and incubated at 25 °C for 8 mins. The wavelength of BSA was excited at 280 nm and emitted at 346 nm.[45] The Stern-Volmer equation (Equation 4) was used to get the K_{sv} constant:

$$\frac{I_0}{I} = 1 + K_q\tau_0[Q] = 1 + K_{SV}[Q] \quad (4)$$

where I_0 and I are the fluorescence intensities in the presence and absence of the quencher, respectively, and K_q, K_{sv}, τ_0, [Q] are the BSA quenching rate constant, dynamic quenching constant, the average lifetime of BSA without the quencher (τ_0 = 10^{-8} s), and quencher concentration respectively.

RESULTS and DISCUSSION

Synthesis and Characterization of L1–L3 and complexes 1a–3a, 1b–3b, 1c–3c

Ligands **L1–L3** were synthesized by reacting 3-pyridinecarboxaldehyde with various substituted aromatic amines in anhydrous ethanol. Ligands **L1**, **L2** and **L3** were of fair to good yields at 72, 55, and 90%, respectively, and are all air-stable and soluble in ethanol, dichloromethane, dimethyl sulfoxide, acetonitrile, chloroform, and acetone. The Schiff bases were characterized using ^{1}H NMR, ^{13}C NMR, FT-IR, Mass and UV-Vis spectroscopy. In the IR spectra of ligands **L1-L3**, sharp peaks between 1619 and 1644 cm^{-1} were assigned to imine ν(C=N), a feature of a Schiff base ligand. The ^{1}H NMR spectra of **L1**, **L2** and **L3** in acetone-*d6* exhibit singlets between 8.81, 8.72 and 8.69 ppm, respectively (Table S1) assigned to the imine proton (CH=N).

Complexes **1a–3a**, **1b–3b** and **1c–3c** were prepared by reacting each ligand **L1–L3** with $AgNO_3$, $AgClO_4$ and $AgCF_3SO_3$, respectively in 2:1 stoichiometry (L:M) in anhydrous ethanol. The complexes were produced in good to excellent yields ranging from 64 to 97% and were stable in the air. Various spectroscopic and analytical techniques were used to establish the complexes' formation and purity. The synthetic process for complexes **1a–3a**, **1b–3b** and **1c–3c** is shown in Scheme 1.

To follow ligand **L1–L3** coordination mode, the ^{1}H-NMR spectra of their protons near the donor atoms were compared to their respective complexes. In the ^{1}H-NMR spectra of complexes **1a–3a**, **1b–3b** and **1c–3c**, the integration values revealed the imine protons resonate between 8.72 and 8.81 ppm showing no notable chemical shift when compared to their free ligands **L1**, **L2** and **L3** chemical shift at 8.81, 8.72, 8.69 ppm respectively. On the other hand, the alpha protons on the pyridine ring of **L1**, **L2** and **L3** show chemical shifts at 8.64, 8.71 and 8.68 ppm, respectively, and on coordination (complexes **1a–3a**, **1b–3b** and **1c–3c**) shifted downfield and resonated between 8.69 and 8.75 ppm suggesting the deshielding of the alpha protons in the pyridine ring by 0.01-0.07 ppm upon coordination to Ag(I). This suggests that **L1–L3** coordinate to the Ag(I) ion *via* the N_{py} atom alone, forming discrete mononuclear complexes **1a–3a**, **1b–3b** and **1c–3c**. This agrees with the reported Ag(I) complexes mode coordination of similar ligands.[46] The formation of **1a–3a**, **1b–3b** and **1c–3c** was also confirmed by correlating their FT-IR spectra with **L1–L3** (Table S1). In the spectra of **1a–3a**, **1b–3b** and **1cv3c**, the position of the -C=N- stretching frequencies remained nearly at the same frequency relative to their ligands, implying the non-involvement of the imine nitrogen atom in coordination with the Ag(I) ion. In contrast, the absorption bands attributed to the pyridinyl N atom between 1568 and 1581 cm^{-1} red-shifted between 1576 and 1595 cm^{-1} compared to their free ligand in **1a–3a**, **1b–3b** and **1c–3c**. This implies that the coordination of **L1–L3** to Ag(I) occurred through the N_{py} donor atom.[47] The UV-Vis spectra of **L1–L3**, **1a–3a**, **1b–3b** and **1c–3c** (Figure 1) were recorded in acetonitrile at room temperature. The spectra of **L2** and **L3** showed π→π* transitions relative to the pyridinyl ring between 235 and 292 nm and imine n→π* transitions between 324 and 325 nm. **L1** has three absorption bands at 288, 348 and 360 attributed to the pyridinyl ring π→π*, imine π→π* and imine n→π* nm transitions.[48,49,50] The absorption patterns of complexes **2a**, **2b**, **2c**, **3a**, **3b** and **3c** are similar, having two absorption bands between 324 and 329 nm attributed to the imine n–π* transition and between 234 and 289 nm allied to the pyridinyl π–π* transition. Complexes **1a**, **1b** and **1c** have three absorption bands. The first absorption band lies between 290 and 292 nm, the second between 348 and 349 nm, and the third is between 356 and 359 nm. These bands are due to the intra-ligand n–π* and π–π*and metal to ligand charge transfer transitions. Relative to their free ligands, the n→π* transitions redshifted in the absorption spectra of **1a**, **1b**, **1c**, **2a**, **2b** and **2c**, while in complexes **3a**, **3b**, and **3c**, a slight blue shift was observed. In the mass spectra of **1a–3a**, **1b–3b** and **1c–3c**, molecular ion peaks m/z = 504 for **1a**, **1b** and **1c** correlating to $[Ag(\mathbf{L1})_2]^+$, while for **2a**, **2b** and **2c** and **3a**, **3b** and **3c** base peaks relating to $[Ag(\mathbf{L2})_2]^+$

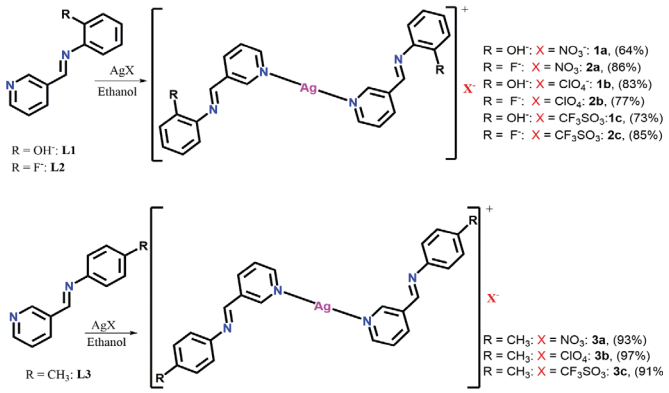

Scheme 1: Formation of complexes **1a–3a, 1b–3b, 1c–3c** under constant magnetic stirring in anhydrous ethanol

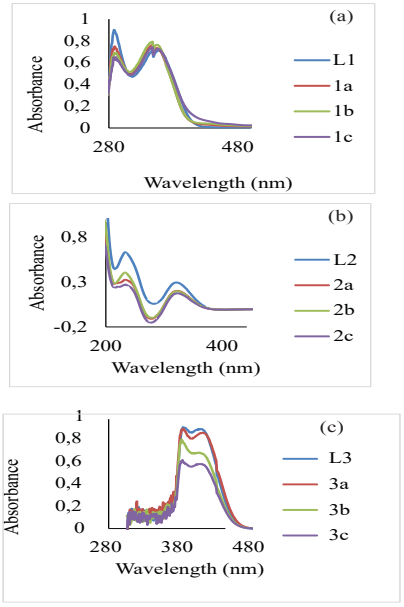

Figure 1: Electronic absorption spectra of (a) **L1** and complexes **1a**, **1b** and **1c**, (b) **L2** and complexes **2a, 2b** and **2c,** (c) L3 and complexes **3a, 3b** and **3c**

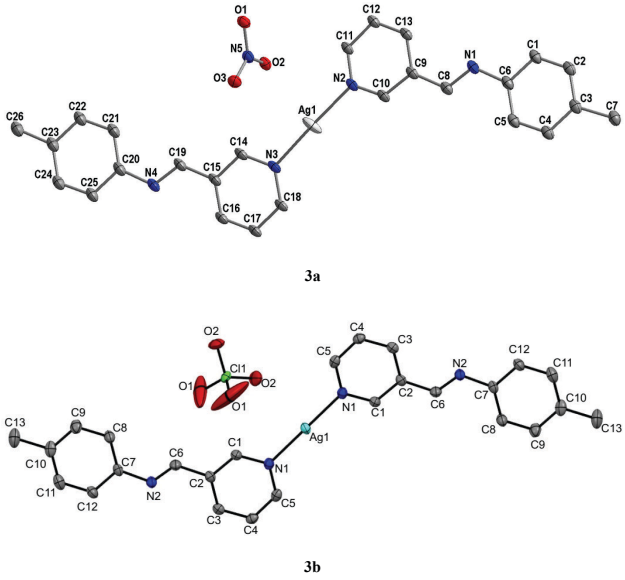

Figure 2: The ORTEP diagrams showing the atom numbering scheme with the thermal ellipsoids drawn at the 50% probability level for molecules **3a** and **3b**. Hydrogen atoms were omitted for clarity

and $[Ag(\mathbf{L3})_2]^+$ were observed at m/z 509 and m/z 501 respectively (Table S2). The formation and purity of the reported structures in scheme 1 were confirmed using all the spectroscopic studies, as well as microanalysis (see ESI Table S1 and Table S2).

Crystal structures of complexes $[Ag(L3)_2]NO_3$ (3a) and $[Ag(L3)_2]ClO_4$ (3b)

The *ORTEP* diagrams and the atom numbering scheme for complexes **3a** and **3b** are shown in Figure 2. Complex 3a asymmetric unit has ten molecules of (E)-1-(pyridin-3-yl)-N-(p-tolyl)methanimine ligands, five Ag(I) ions and five nitrate anions, whereas complex **3b** contains half a molecule of the cation $[Ag(\mathbf{L3})]^+$ and half a molecule of the perchlorate anion. In both complexes, the cations are essentially planar in conformation. Around the Ag(I) ion, the complexes have a distorted linear geometry in which only the pyridine N atoms are involved in coordination with the Ag(I) center, with N—Ag—N bond angles ranging from 175.0(4) to 180° (Table 2). The anion molecules in both complexes are outside the coordination spheres. The angle around the Ag(I) centers in complexes **3a** and **3b** is similar to that of reported silver(I) complexes.[51]

In-vitro antimicrobial studies

Several antimicrobial agents have been used to treat infectious diseases[52], yet multidrug-resistant bacteria pose a serious global health threat. The *S. typhi*, *P. aeruginosa*, *E. coli*, *K. pneumoniae*, Methicillin-resistant *S. aureus* and *S. aureus* bacteria selected in this study cause various human infections and diseases such as typhoid fever, gastroenteritis, urinary tract infections, respiratory system infections, soft tissue infections, neonatal meningitis, pneumonia, skin infections and endocarditis.[53,54] These bacteria prove difficult to treat and tend to develop resistance to antimicrobial agents quickly, making antimicrobial agents less effective. Therefore, developing efficient novel molecules as a potential antimicrobial agent is crucial. The antibacterial activity of ligands; **L1–L3**, silver(I) complexes; **1a–3a**, **1b–3b**, **1c–3c**, Ciprofloxacin (used as a control), and three silver salts was assessed against six bacteria strains using the minimum inhibitory concentration technique (MIC in μg mL^{-1}). Table 3 lists the observed MIC values of the compounds.

Table 2: Selected geometric parameters for complexes [Ag(L3)2]NO3 (**3a**) and [Ag(L3)2]ClO4 (**3b**)

	3a	3b
Ag—Npy	2.168(9) 2.171(7) 2.184(9) 2.171(7)	2.162(19) 2.162(19)
Npy—Ag—Npy	175.9(4) 178.0(4)	180

The antibacterial activities of the free ligands revealed **L2** to be the least active ligand as it showed activity only against *P. aeruginosa* with 1000 μg mL^{-1} MIC value. **L1**, on the other hand, is selectively active against *S. aureus* and *P. aeruginosa* only, and **L3** is active against *P. aeruginosa* and *E. coli* only. From the MIC values obtained for complexes **1a–3a**, **1b–3b** and **1c–3c** against *S. aureus*, all the complexes except **1c**, **2b**, **3a** and **3b** showed better activity (1.6-12.5 μg mL^{-1}) with respect to the reference standard (25 μg mL^{-1}). **3c** (with CH_3 substituent) had the best activity than the reference standard and the metal salts against *S. aureus*. Similarly, almost all the complexes displayed significant activity against MRSA. MIC values between 0.025 and 12.5 μg mL^{-1} were recorded for all the complexes except **1a**, **2a**, **2b** and **3a** with 50-1000 μg mL^{-1} MIC against MRSA. These MIC results of the complexes against *S. aureus* and MRSA showed that most of the complexes had better activity than the reference standard towards gram-positive bacteria.

Towards the gram-negative bacteria, the complexes showed fair activities against *P. aeruginosa* with only **3a** (with methyl substituent and NO_3^- as an anion) having a lower MIC (0.1 μg mL^{-1}) than the reference standard (0.2 μg mL^{-1}). **3b**, also with methyl substituent, had the same MIC (0.2 μg mL^{-1}) as the reference standard, and **2b** (0.8 μg mL^{-1}) had similar activities as the $AgClO_4$ against *P. aeruginosa*. Against *S. typhi*, only complex **1c** (with OH substituent and $CF_3SO_3^-$) had similar activity as the reference standard, while **2b** and **2c**, each with 6.25 μg mL^{-1} MIC had better activity than the $AgNO_3$ and $AgCF_3SO_3$ salts against *S. typhi*. For the antimicrobial activities of the complexes against *E. coli*, **2b** and **3b** displayed better activity, with each of their MIC values (0.25-0.4 μg mL^{-1}) lower than the reference standard (1.6 μg mL^{-1}). **2c** had the same MIC as the standard against *E. coli*. The activity of **3c** with methyl substituent (0.4 μg mL^{-1}) is double that of the standard (0.8 μg mL^{-1}) against *K. pneumoniae*, while the activity of **2b** (with F^-) against *K. pneumoniae* is the same as that of $AgClO_4$. Each of the complexes with better antimicrobial activity has either CH_3 or F^- substituent. This shows that F^- and CH_3 substituents and ClO_4^- and $CF_3SO_3^-$ anions play a role in the complexes' antimicrobial activity.

In general, all the complexes were fairly active against the tested bacteria strains in comparison with the standard, with **3c** (with methyl substituent) somewhat showing notable antimicrobial activity against all the bacteria tested. Significant antimicrobial activity of compounds with methyl substituents [55,56] have been reported.

Overall, the coordination of ligands **L1–L3** to the silver(I) ion impacted their antibacterial activity, as proven by the MIC values recorded. The improved antibacterial activity of the studied complexes can be linked to the mechanism of action of the silver(I) ion, where the silver(I) ion is slowly released from the ligand upon entry into the bacteria cell to interact with nucleic acids, protein thiol groups and several vital enzymes. This leads to protein denaturation, membrane malfunction, cell division blockage, and consequently, inhibiting the organism's growth.[35] Chelation, known for the promotion of π–electron delocalization along a chelate ring and complexes lipophilicity increment, could have encouraged the complexes' absorption into the bacterial membranes and inhibited the metal-binding sites in microbial enzymes.[57] The impact of the perchlorate and triflate anions, as well as the F^- and CH_3 substituents on the complexes' antibacterial activity, were also identified, which correlates with that of the literature.[55,56] Relative to MIC values between 4 and 256 μg mL^{-1} of similar Ag(I) complexes reported,[58,59,60] the Ag(I) complexes in this study demonstrated better antibacterial activity with MIC values between 0.2 and 100 μg mL^{-1}.

Antioxidant study

Synthetic antioxidants can slow down or stop the damage to DNA, RNA and protein substrates caused by free radicals; they can also be used for stabilizing organic materials against degradation, such as additives in polymer formulations.[61] The antioxidant activity of **L1–L3** and **1a–3a**, **1b–3b** and **1c–3c** were studied by the ferric reducing antioxidant power (FRAP) method. The FRAP assay is based on an antioxidant's capacity to reduce Fe(III) tripyridyltriazine complex to Fe(II) tripyridyltriazine complex.[62] The compounds' 50% inhibitory concentrations (IC_{50} in mg mL^{-1}) are used to express the antioxidant activity of the compounds. Ascorbic acid was utilized as a control, and its IC_{50} value was 2.68 mg mL^{-1}. The IC_{50} values for **L1–L3** and complexes **1a–3a**, **1b–3b** and **1c–3c** are displayed in Table 4, and Figure 3 displays a histogram of the free radical scavenging activity *vs.* conc. (mg mL^{-1}).

Ligands **L1**, **L2** and **L3** had 1.07, 10.00 and 13.44 mg mL^{-1} IC_{50}, respectively, depicting **L1** (with a hydroxyl group) as a good antioxidant compared to the reference IC_{50} of 2.68 mg mL^{-1}. A further evaluation of the complexes' antioxidant activity revealed the complexes displayed higher antioxidant activities than the free ligands. Among all the complexes, **1a**, **1b**, **1c**, and **3c** exhibited significant antioxidant activity, with IC_{50} values ranging from 0.86 to 2.47 mg mL^{-1} (Table 4). These complexes demonstrated greater activity than ascorbic acid, whose capacity to reduce Fe(III) to Fe(II) is shown by an IC_{50} value of 2.68 mg mL^{-1}. Most of these complexes with notable antioxidant activity have a phenolic ligand, which could have influenced their antioxidant property. This observation can be compared with El Jemli et al. 2016[64] reports, where phenolic compounds were identified with high antioxidant activity.

Anticancer studies

Transition metal complexes have gained more recognition as promising anticancer agents than platinum-based complexes previously employed. Therefore, this study used an MTT cell viability assay to ascertain the anticancer effects of complexes **3a**, **3b**, **3c** and Cisplatin against HEK293, A375, HELA and MDA-MB231. The concentration of the complexes necessary to kill 50% of the cells and the selectivity index (SI) was determined and tabulated in Table 5. The results indicate that **3a**, **3b**, and **3c** showed antiproliferative effects on HELA with EC_{50} values of 44.21 ± 1.87, 32.14 ± 3.91 and 28.07 ± 3.09 μM, respectively, better than Cisplatin (EC_{50} > 50 μM). The impact of the methyl group of the complexes on their remarkable

Table 3: Minimum inhibitory concentration (μg mL^{-1}) of pyridinyl Schiff bases (**L1–L3**) and their Ag(I) complexes (**1a–3a, 1b–3b** and **1c–3c**)

Cmp	*Staphylococcus aureus*	Methicillin-resistant *S. aureus*	*Pseudomonas aeruginosa*	*Salmonella typhimurium*	*Escherichia coli*	*Klebsiella pneumoniae*
L1	1000	**	1000	**	**	**
L2	**	**	1000	**	**	**
L3	**	**	1000	**	1000	**
1a	6.25	50	6.25	100	12.5	12.5
2a	12.5	1000	12.5	25	6.25	6.25
3a	50	1000	0.1	12.5	12.5	3.125
1b	12.5	6.25	25	12.5	12.5	12.5
2b	50	1000	0.8	6.25	0.4	1.6
3b	100	0.025	0.2	50	0.25	12.5
1c	1000	12.5	1000	0.4	1000	1000
2c	12.5	12.5	12.5	6.25	1.6	6.25
3c	1.6	0.2	3.125	12.5	6.25	0.4
SN	3.125	0.2	12.5	1000	0.8	1000
SP	3.125	6.25	0.8	0.2	25	1.6
ST	**	1000	1000	12.5	50	1000
S	25	25	0.2	0.4	1.6	0.8

Cmp = compounds, **= inactive, S = Ciprofloxacin, SN = silver nitrate, SP = silver perchlorate,
ST = silver triflate, n = 3

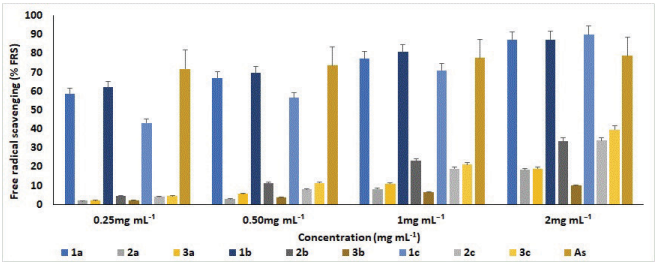

Figure 3: Percentage radical scavenging against concentration (mg mL^{-1}) of complexes **1a–3a**, **1b–3b** and **1c–3c** and ascorbic acid. As = ascorbic acid, n = 3

Table 4: The ferric reducing antioxidant power of **L1–L3** and complexes **1a–3a**, **1b–3b** and **1c–3c**

LIGAND/COMPLEXES	IC_{50} (mg mL^{-1})
Ascorbic acid[63]	2.68 ± 0.11
L1	1.07 ± 0.0016
L2	10.00 ± 0.0093
L3	13.44 ± 0.013
1a	0.88 ± 0.002
2a	5.66 ± 0.0071
3a	5.09 ± 0.0087
1b	0.86 ± 0.0043
2b	2.74 ± 0.0068
3b	9.19 ± 0.016
1c	0.91 ± 0.0076
2c	2.90 ± 0.004
3c	2.47 ± 0.0077

As = ascorbic acid, n = 3

cytotoxicity against HELA can be related to that of Sreelatha et al. 2014[65] who reported the significance of the methyl group in the cytotoxicity of naphthoquinone amide derivatives towards HELA. The type of counter ion present in the complex was also observed to have influenced their cytotoxicity as **3c** (with $CF_3SO_3^-$ anion) had better cytotoxicity, followed by **3b** (with ClO_4^- anion) and **3a** (with NO_3^- anion) against the HELA. While **3a** and **3b** showed poor cytotoxicity when compared to Cisplatin (EC_{50} = 22.68 ± 4.89 μM) against MDA-MB231, the concentration of 3c (EC_{50} = 23.30 ± 3.82 μM) used to kill 50% of the cells was almost similar to that of Cisplatin. Against A375, **3a**, **3b** and **3c** with EC_{50} between 33.73 ± 5.83 and 62.02 ± 7.23 μM showed low cytotoxicity when compared to Cisplatin with 3.4 ± 0.5μM EC_{50} value. The selectivity index of the complexes was determined as the quotient obtained by dividing the HEK293 EC_{50} value by the EC_{50} value of the respective cancer cell lines. In comparison to Cisplatin, all the complexes displayed poor selectivity for A375, HELA and MDA-MB231 cancer cells, according to the SI data in Table 5. This indicates that the complexes cannot selectively inhibit the growth of the cancer cells without attacking the normal cell.

DNA binding studies

In designing potential bioactive drugs, the interaction of such drug molecules with DNA is important since DNA is the primary target for most biological agents. The electronic absorption titration was used to follow the interactions of **L1–L3**, **1a–3a**, **1b–3b** and **1c–3c** with CT-DNA; significant absorption bands between 274 and 277 nm attributed to the $\pi \rightarrow \pi^*$ transition energy were observed for the compounds. The absorption spectra of the compounds further showed a hypochromic shift between 6.34 and 58.62% and a bathochromic shift between 2 and 5 nm except for **1a, 3c, 4b** and **4c** with hypochromic and slight hypsochromic shifts. The hypochromic shift indicates the compounds bind in a non-covalent intercalative fashion to the CT-DNA double helix.[66] The hypochromic absorption spectra of the compounds in the presence and absence of CT-DNA are displayed in Figures 4a and S49–S59 (see ESI).

The "K_b" representing the binding constants of the compounds was determined using the Wolfe-Shimer equation (Eq. ii) by finding the ratio of the slope to the intercept from the plot of [DNA]/($\varepsilon_a - \varepsilon_f$) versus [DNA] to compare quantitatively the affinity of **L1–L3**, **1a–3a**, **1b–3b** and **1c–3c** toward CT-DNA. The binding constant of ligands **L1–L3** was found to be between 1.33 × 10^4 and 2.85 × 10^5, while **1a–3a**, **1b–3b** and **1c–3c** were found to be between 2.33 × 10^5 and 3.00 × 10^6 M^{-1}(Table 6). The K_b value is proportional to the compounds' binding affinity and intercalative strength when it binds to DNA. Therefore, the ligands have poor interactions with CT-DNA not until their coordination to Ag(I) ion, which improves their binding affinity. Comparing the K_b value of the complexes, **1b** (3.00 × 10^6 M^{-1}) had the highest binding affinity (Figure 4a), followed by **1c** with 1.75 × 10^6 M^{-1}.

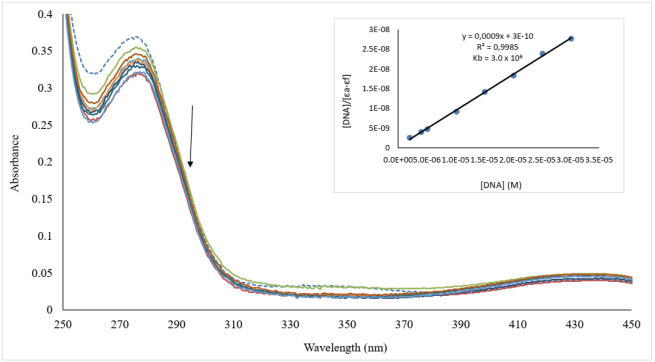

Figure 4a: UV-Vis Spectra of complex 1b at 5.0 × 10^{-5} M in the absence (dotted line) and the presence of CT-DNA (0–3.0 × 10^{-5} M) at 275 nm λ_{max}. A Stern-Volmer plot of **1b** interaction with CT-DNA is shown in the inset

Table 6: K_b, K_{sv}, K_q, and K_{bin} constant and n values obtained from the interactions of complexes **1a–3a**, **1b–3b** and **1c–3c** with CT-DNA and BSA

Cmp.	Cmp.-CT-DNA		EB-CT-DNA BINDING				BSA -Complex				
	K_b (M^{-1}) × 10^5	R^2	K_{sv} (M^{-1}) × 10^4	K_q ($M^{-1}S^{-1}$)× 10^{12}	K_{bin} (M^{-1}) × 10^5	n	K_b (M^{-1}) × 10^4	K_{sv} (M^{-1})× 10^4	K_q ($M^{-1}S^{-1}$) × 10^{12}	K_{bin} (M^{-1}) × 10^4	n
1a	6.00	0.99	4.39	4.39	3.37	1.19	3.99				
2a	2.67	0.99	2.38	2.38	2.27	1.14	16.8	2.44	2.44	5.55	1.08
3a	3.33	0.99	3.88	3.88	4.62	1.23	3.40				
1b	30.00	0.99	4.52	4.52	1.25	1.10	17.2				
2b	2.33	0.96	3.54	3.54	1.55	1.14	2.30	2.00	2.00	2.60	1.02
3b	2.75	0.98	2.68	2.68	5.03	1.27	36.7				
1c	17.50	0.99	1.61	1.61	8.57	1.34	3.11				
2c	4.00	0.99	4.07	4.07	2.11	1.15	17.2	1.62	1.62	1.36	0.99
3c	5.00	0.99	4.42	4.42	9.57	1.28	4.52				
L1	2.85	0.95									
L2	1.33	0.99									
L3	1.33	0.98									

R = correlation coefficient

Table 5: EC50 (μM) and SI data of Cisplatin, **3a**, **3b** and **3c** against A375, HELA and MDA-MB231

Complex	EC_{50} ± SD (μM)				SI		
	HEK293	HELA	MDA-MB231	A375	HELA	MDA-MB231	A375
Cisplatin	14.2 ± 3.8	>50	22.68 ± 4.89	3.4 ± 0.5	0.28	0.63	4.17
3a	7.29 ± 1.09	44.21 ± 1.87	55.21 ± 3.76	62.02 ± 7.23	0.16	0.13	0.12
3b	7.99 ± 1.88	32.14 ± 3.91	46.17 ± 4.88	57.64 ± 3.92	0.25	0.17	0.14
3c	7.03 ± 2.10	28.07 ± 3.09	23.30 ± 3.82	33.73 ± 5.83	0.25	0.30	0.21

SD = standard deviation, n = 3

The strong binding affinity of these two complexes (**1b** and **1c**) to CT-DNA could have been related to the hydroxyl group present in the complexes, similar to that of the literature.[67]

Fluorescence competitive displacement studies

The binding mode of **1a–3a**, **1b–3b** and **1c–3c** to CT-DNA was further ascertained using the fluorescence competitive displacement experiments. It is worth mentioning that **L1–L3** were exempted from this analysis since their CT-DNA binding affinity is lower than that of the complexes. The fluorescence competitive displacement investigation is based on the test complexes displacing ethidium bromide (an intercalative agent) from the CT-DNA-EB adduct. While performing the experiment, the gradual introduction of **1a–3a**, **1b–3b** and **1c–3c** to ethidium bromide incubated with CT-DNA resulted in a significant reduction in the CT-DNA-EB fluorescence intensity at 605 nm (Figures 4b and S60–S67). This means the complexes could displace CT-DNA-bound EB and bind to CT-DNA at the intercalation site, thus validating the complexes binding to CT-DNA *via* intercalation mode.

The quenching strength, K_{sv}, was then computed from the slope of the linear quenching plot of F_o/F versus the concentration of the complexes (Equation 3) to measure the relative binding interaction of the complexes with CT-DNA. The K_{sv} values for **1a–3a**, **1b–3b** and **1c–3c** ranged from 1.61 to 4.52 × 10^4 M^{-1} (Table 6), demonstrating their high affinity for CT-DNA. The maximum binding affinity to CT-DNA was found in complex **1b** (Figure 4b), which corresponds to the complex with the highest intrinsic K_b constant (Figure 4a). The quenching of the fluorescence intensity of EB-CT-DNA adduct by the complexes was further utilized to evaluate the quenching mechanism (K_q), binding constant (K_{bin}) and the binding sites (n). The quenching mechanism, which could either be static or dynamic, due to the obtained Stern-Volmer linear plots of the complexes (inset Figures 4b and S60–S67), can be evaluated from Equation 5.

$$K_q = \frac{K_{SV}}{\tau_o} \quad (5)$$

K_{sv} and K_q represent the Stern-Volmer quenching constant and bimolecular quenching constant, respectively, while τ_0 represents an average fluorophore lifetime in the absence of the quencher, usually 10^{-8} s in biomacromolecules. The K_q of the complexes was determined to be between 1.61 and 4.52 × 10^{12} $M^{-1}S^{-1}$ (Table 6), which is higher than the maximal diffusion collision quenching rate constant of many biological macromolecule quenchers (2 × 10^{10} $M^{-1}S^{-1}$).[68] The range of the K_q value obtained indicates that the quenching by **a–3a**, **1b–3b** and **1c–3c** was caused by a static quenching mechanism and that complexes formed between quenching and fluorescent molecules are stabilized at the ground state.[69] The K_{bin} of complexes **a–3a**, **1b–3b** and **1c–3c** with CT-DNA were calculated using the double-logarithmic (Equation 6), where a plot of log F_0 – F/F vs log [Q] of complexes **1a–3a**, **1b–3b** and **1c–3c** yielded a straight line with a slope of n and y-axis intercept of log K_{bin} (Figures S68–S75)

$$\log\frac{F_0 - F}{F} = \log K_{bin} + n\log[Q] \quad (6)$$

The relative fluorescence intensities of CT-DNA in the absence and presence of the quencher, respectively, are represented by F_0 and F. At the same time, [Q] is the quencher concentration, K_{bin} is the binding constant, and n is the number of binding sites. The values of n for complexes **a–3a**, **1b–3b** and **1c–3c** are all close to 1, indicating that all complexes bind to one reactive site on the CT-DNA, as shown in Table 6. With a binding constant (K_{bin}) equal to 9.57 × 10^5 M^{-1}, Complex **3c** (Figure 4c) had the highest binding affinity to CT-DNA.

Protein binding studies

Drug molecules are transported well by proteins found in blood plasma. Therefore, the mechanism of protein interactions with a potential drug plays a fundamental role in understanding such drug pharmacokinetics and pharmacodynamics.[70] The protein standard in this work was BSA, which was utilized to understand the pharmacokinetics and pharmacodynamics of **a–3a**, **1b–3b** and **1c–3c**. The interaction between **a–3a**, **1b–3b** and **1c–3c** and BSA were explored by fluorescence and electronic absorption spectroscopy. For the fluorescence assay, the excitation of BSA at 280 nm resulted in its emission between 300 and 400 nm, which can be attributable to the amino acid residues such as tyrosine (Tyr), tryptophan (Trp) and phenylalanine (Phe).[71] As observed in the emission spectra of the compounds, the incremental addition of **2a**, **2b** and **2c** to a constant concentration of BSA led to hypochromic shifts between 15.99 and 23.59% (an indication of complex formation) with the fluorescence intensity of the BSA around 350–360 nm with a slight redshift between 1 and 3 nm in the maximum emission. These findings suggest a complex formation between the BSA and studied compounds leading to the quenching of the BSA. The emission spectra of BSA in the presence of **2a**, **2b** and **2c** are shown in Figure 5a and Figures S79 and S82. **2a** (Figure 5a) quenched the intrinsic fluorescence of BSA more. BSA's fluorescence intensity was not quenched by complexes **1a**, **1b**, **1c**, **3a**, **3b** and **3c**. The presence of either OH^- or CH_3 in **1a**, **1b**, **1c**, **3a**, **3b** and **3c** could have limited their ability to access the protein's binding site buried in the hydrophobic environment. Non-binding interaction of BSA with similar substituents has been reported by our group.[72] The possible quenching mechanism of the BSA fluorescence by **2a**, **2b** and **2c** was determined by the Stern-Volmer Equation (Equation 4). The slope of the linear regression on the Stern–Volmer plot of I_0/I vs [Q] yielded the K_{sv} values for the complexes, and the K_q value was determined using the equation:

$$K_q = \frac{K_{SV}}{\tau_o}$$

The K_{sv} and K_q values were found to be between 1.62 × 10^4 and

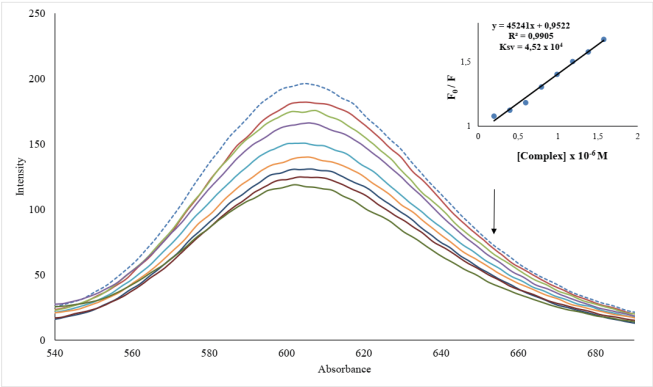

Figure 4b: Fluorescence spectra of EB-CT-DNA in the absence (dotted line) and the presence (solid line) of complex **1b**. A Stern-Volmer plot of **1b** interaction with EB-CT- DNA is shown in the inset.

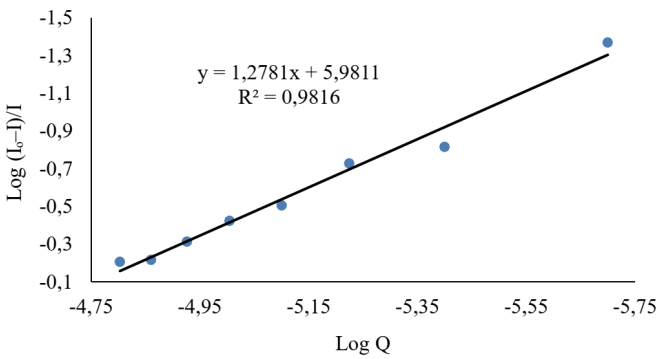

Figure 4c: Complex **3c** double-logarithmic plot

2.44×10^4 M^{-1} and 1.62×10^{12} and 2.44×10^{12} M^{-1}, respectively. The calculated K_q values were higher than the biomolecules' maximum scatter collision-quenching constant (2×10^{10} M^{-1} S^{-1}), indicating that the complexes' BSA quenching mechanism is static. Scatchard Equation vii can be used to calculate the binding constant (K_{bin}) and the number of binding sites (n) for static quenching:

$$\log \frac{I_0 - I}{I} = \log K_{bin} + n \log[Q] \quad (7)$$

The slope and intercept of the double logarithm regression of $\log(I_0 - I)/I$ versus $\log[Q]$ (Figure 5b and Figures S84–S85) can be used to compute n and $K_{bin,}$ respectively. The K_{bin} values indicate that BSA has a modest affinity for the complexes. The maximum binding affinity for BSA was found in Complex 2a (Figure 5b). The number of the binding site (n) for complexes **2a**, **2b** and **2c** are about one, implying that one molecule of each complex binds to BSA. The results obtained in this study reveal moderate interactions between these Ag(I) complexes and BSA, which occur through hydrophobic force and static mechanism.

In the electronic absorption spectroscopy titration, each addition of complexes 1a–3a, 1b–3b and 1c–3c to a constant BSA concentration led to an increase in the BSA λ_{max} at ~280 nm with slight redshifts (Figure 5c and Figures S86–S93). The intercept-to-slope ratio of the linear curve of a plot of $1/[A - A_0]$ vs $1/[complex]$ yielded the K_b constant in this case. The complexes' K_b value falls between 2.30×10^4 and 3.67×10^5 M^{-1} (Table 5), which is similar to Anjomshoa et al. 2014[43] binding constant values between 10^4 and 10^6 M^{-1}. The maximum binding affinity for BSA was found in complex **3b** (Figure 5c). A similar literature report[73] can be linked to the effect of **3b** ligand substituents on their binding affinity to BSA.

CONCLUSION

Nine sets of mononuclear discrete Ag(I) complexes of aryl substituted (*E*)-*N*-phenyl-1-(pyridin-3-yl)methanimine were synthesized, characterized and bio-evaluated for antibacterial, antioxidant and anticancer activities as well as their binding with biomolecules. Based on the spectral evidence, the ligands coordinated to the Ag(I) center in a 2:1 stoichiometry (L:M) through the nitrogen atom of the pyridine only, with complexes **3a** and **3b** having a linear geometry around the Ag(I) center as obtained from the single crystal X-ray diffraction analysis. The biological evaluations of the complexes reveal their structural activity relationship. From the antibacterial screening, complexes possessing either CH_3 or F^- substituent showed remarkable activity against the tested microorganisms. The remarkable impact of the ClO_4^- and $CF_3SO_3^-$ anions on the complexes' antibacterial activities was also observed. The results of the antioxidant study by the FRAP method showed that complexes with OH^- substituent exhibit good antioxidant activity with reference to ascorbic acid. UV–Vis absorption and fluorescence spectroscopy were used to investigate the complexes' interactions with CT-DNA and BSA. The binding studies of the Ag(I) complexes with CT-DNA suggested their intercalative mode of interaction. The high K_b constant value revealed that all the complexes had a high binding affinity for CT-DNA. All the complexes exhibit significant binding affinity to BSA, and the fluorescence quenching of the BSA by the Ag(I) complexes were initiated by a static mechanism. The moderate to high binding affinities of the Ag(I) complexes with CT-DNA and BSA denotes that the novel Ag(I) complexes can bind to DNA and serum albumin. The complexes showed potential anti-cervical cancer activity. Hence, the Ag(I) complexes are potential therapeutic alternatives since their remarkable antimicrobial, antioxidant and anticancer activities were recorded.

CONFLICT OF INTEREST

No potential conflict of interest was reported by the authors.

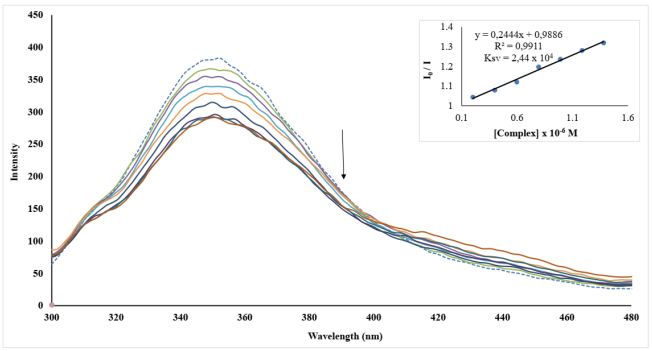

Figure 5a: BSA fluorescence emission spectra in the absence (dashed line) and the presence (solid line) of a different concentration of complex **2a**. A Stern-Volmer plot of **2a** interaction with BSA is shown in the inset

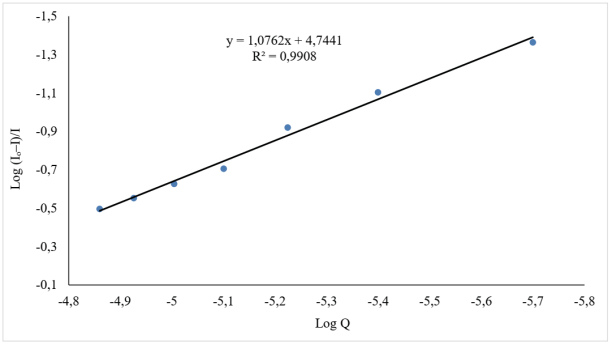

Figure 5b: BSA–Complex **2a** interactions in a double-logarithmic plot

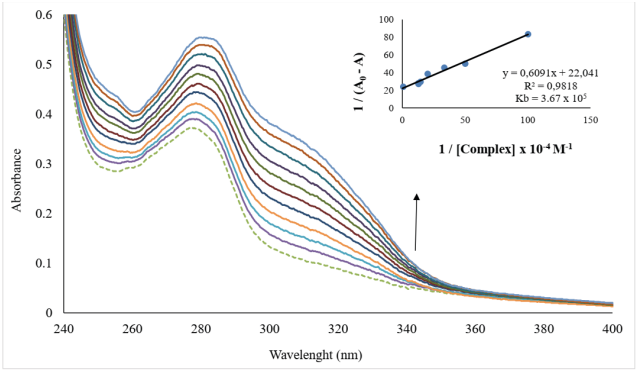

Figure 5c: Electronic absorption spectra of BSA in the absence (dashed line) and the presence (solid line) of various concentrations of complex **3b**. A plot of $1/(A_0 - A)$ vs. $1/Complex] \times 10^{-4}$ M^{-1} is shown in the inset

AUTHORS CONTRIBUTION

All authors contributed to the preparation of this manuscript. BO provided the resources and supervised the project. AAA synthesized, characterized the metal complexes and carried out the biological studies of the complexes. KO and VFS did the antioxidant analysis. AAA wrote the original draft. BO and Md.SI reviewed the manuscript.

FUNDING

The authors are grateful for financial support from the National Research Foundation of South Africa (Grant number: 119342).

ACKNOWLEDGMENTS

The authors appreciate the help and use of the facilities from the University of KwaZulu-Natal, South Africa.

SUPPLEMENTARY MATERIAL

Supplementary information for this article is provided in the online supplement.

ORCID IDs

Adesola A. Adeleke: https://orcid.org/0000-0001-9287-5960
Md. Shahidul Islam: https://orcid.org/0000-0003-0309-9491
Kolawole Olofinsan: https://orcid.org/0000-0002-2987-0996
Veronica F. Salau: https://orcid.org/0000-0002-3796-4992
Bernard Omondi: https://orcid.org/0000-0002-3003-6712

REFERENCES

1. Vhanale BT, Deshmukh NJ, Shinde AT. Synthesis, characterization, spectroscopic studies and biological evaluation of schiff bases derived from 1-hydroxy-2-acetonapthanone. Heliyon. 2019;5(11):e02774. https://doi.org/10.1016/j.heliyon.2019.e02774
2. Adeleke A, Omondi B. Crystal structure of a chiral sec-amine, 4-chloro-n-(1-(pyridin-2-yl)ethyl)aniline. Molbank. 2022;2022(1). https://doi.org/10.3390/m1335
3. Adeleke A, Zamisa SJ, Omondi B. Crystal structure of 4-(1-phenylimidazo[1,5-a]pyridin-3-yl)benzoic acid ($C_{20}H_{14}N_2O_2$). Zeitschrift für Kristallographie - New Crystal Structures. 2019;234(6):1157-1159. https://doi.org/10.1515/ncrs-2019-0300
4. Gupta K, Sutar AK. Catalytic activities of schiff base transition metal complexes. Coord Chem Rev. 2008;252(12-14):1420-1450. https://doi.org/10.1016/j.ccr.2007.09.005
5. Oiye E, Ribeiro MFM, Katayama JMT, Tadini MC, Balbino MA, Eleoterio IC, Magalhaes J, Castro AS, Silva RSM, da Cruz Junior JW, Dockal ER, de Oliveira MF. Electrochemical sensors containing schiff bases and their transition metal complexes to detect analytes of forensic, pharmaceutical and environmental interest. A review. Crit Rev Anal Chem. 2019;49(6):488-509. https://doi.org/10.1080/10408347.2018.1561242
6. Zhang J, Xu L, Wong W-Y. Energy materials based on metal schiff base complexes. Coord Chem Rev. 2018;355:180-198. https://doi.org/10.1016/j.ccr.2017.08.007
7. Chaturvedi D, Kamboj M. Role of schiff base in drug discovery research. Chem Sci J. 2016;7(2):e114. https://doi.org/10.4172/2150-3494.1000e114
8. Kajal A, Bala S, Kamboj S, Sharma N, Saini V. Schiff bases: A versatile pharmacophore. J Catal. 2013;2013:1-14. https://doi.org/10.1155/2013/893512
9. Zamisa S, Ngubane NP, Adeleke AA, Jonnalagadda SB, Omondi B. Classical intermolecular hydrogen bonding motifs of heterocyclic rac-2-amino-3-carbonitrile derivatives: Linking hirshfeld surface analysis, ct-DNA binding affinity, and molecular docking. Cryst Growth Des 2022;22(10):5814–5834. https://doi.org/10.1021/acs.cgd.1c01514
10. Mendu P, Kumari CG, Ragi R. Synthesis, characterization, DNA binding, DNA cleavage and antimicrobial studies of schiff base ligand and its metal complexes. J Fluoresc. 2015;25(2):369-378. https://doi.org/10.1007/s10895-015-1520-6
11. Nandanwar S, Kim HJ. Anticancer and antibacterial activity of transition metal complexes. ChemistrySelect. 2019;4(5):1706-1721. https://doi.org/10.1002/slct.201803073
12. Pal M, Musib D, Roy M. Transition metal complexes as potential tools against sars-cov-2: An in silico approach. New J Chem. 2021;45(4):1924-1933. https://doi.org/10.1039/D0NJ04578K
13. Levina A, Lay PA. Metal-based anti-diabetic drugs: Advances and challenges. Dalton Trans. 2011;40(44):11675-11686. https://doi.org/10.1039/c1dt10380f
14. Yusuf T, Akintayo DC, Oladipo SD, Adeleke AA, Olofinsan K, Vatshaa B, Mabuba N. The effect of structural configuration on the DNA binding and in vitro antioxidant properties of new copper(II) N_2O_2 schiff base complexes. New J Chem. 2022:1-13. https://doi.org/10.1039/D2NJ01477G
15. Khan S, Nami SAA, Bhat SA, Kareem A, Nishat N. Synthesis, characterization and antimicrobial study of polymeric transition metal complexes of Mn(II), Co(II), Ni(II), Cu(II) and Zn(II). Microb Pathog. 2017;110:414-425. https://doi.org/10.1016/j.micpath.2017.07.008
16. Ndagi U, Mhlongo N, Soliman ME. Metal complexes in cancer therapy - an update from drug design perspective. Drug Des Devel Ther. 2017;11:599-616. https://doi.org/10.2147/DDDT.S119488
17. Hussain A, AlAjmi MF, Rehman MT, Amir S, Husain FM, Alsalme A, Siddiqui MA, AlKhedhairy AA, Khan RA. Copper(II) complexes as potential anticancer and nonsteroidal anti-inflammatory agents: In vitro and in vivo studies. Sci Rep. 2019;9(1):5237. https://doi.org/10.1038/s41598-019-41063-x
18. Ghdhayeb M, Haque RA, Budagumpi S, Khadeer Ahamed MB, Abdul Majid AMS. Mono- and bis-N-heterocyclic carbene silver(I) and palladium(II) complexes: Synthesis, characterization, crystal structure and in vitro anticancer studies. Polyhedron. 2017;121:222-230. https://doi.org/10.1016/j.poly.2016.09.065
19. Tesseromatis C, Alevizou A. The role of the protein-binding on the mode of drug action as well the interactions with other drugs. Eur J Drug Metab Pharmacokinet. 2008;33(4):225-230. https://doi.org/10.1007/BF03190876
20. Karataş M, Günal S, Mansur A, Alıcı B, Çetinkaya E. Synthesis and antimicrobial properties of cycloheptyl substituted benzimidazolium salts and their silver(I) carbene complexes. Heterocycl Comm. 2016;22(6):357–361. https://doi.org/10.1515/hc-2016-0105
21. Roymahapatra G, Mandal SM, Porto WF, Samanta T, Giri S, Dinda J, Franco OL, Chattaraj PK. Pyrazine functionalized Ag(I) and Au(I)-NHC complexes are potential antibacterial agents. Curr Med Chem. 2012;19(24):4184-4193. https://doi.org/10.2174/092986712802430090
22. Gok Y, Akkoc S, Erdogan H, Albayrak S. In vitro antimicrobial studies of new benzimidazolium salts and silver N-heterocyclic carbene complexes. J Enzyme Inhib Med Chem. 2016;31(6):1322-1327. https://doi.org/10.3109/14756366.2015.1132210
23. Melaiye A, Youngs WJ. Silver and its application as an antimicrobial agent. Expert Opin Ther Pat. 2005;15(2):125-130. https://doi.org/10.1517/13543776.15.2.125
24. Wu H, Yuan J, Bai Y, Pan G, Wang H, Kong J, Fan X, Liu H. Synthesis, structure, DNA-binding properties and antioxidant activity of silver(I) complexes containing v-shaped bis-benzimidazole ligands. Dalton Trans. 2012;41(29):8829-8838. https://doi.org/10.1039/c2dt30512g
25. Slimani I, Mansour L, Abutaha N, Harrath AH, Al-Tamimi J, Gürbüz N, Özdemir I, Hamdi N. Synthesis, structural characterization of silver(I)-NHC complexes and their antimicrobial, antioxidant and antitumor activities. J King Saud University - Science. 2020;32(2):1544-1554. https://doi.org/10.1016/j.jksus.2019.12.010
26. Tang X, Qu Y, Zhao K, Wang C, Wu Y, Mao S, Wu H. Synthesis, crystal structure, fluorescence and antioxidant properties of a binuclear Ag(I) complex based on the $spph_3$ ligand. J Chem Res. 2019;43(5-6):184-188. https://doi.org/10.1177/1747519819857503
27. Jehdaramarn A, Pornsuwan S, Chumsaeng P, Phomphrai K, Sangtrirutnugul P. Effects of appended hydroxyl groups and ligand chain length on copper coordination and oxidation activity. New J Chem. 2018;42(1):654-661. https://doi.org/10.1039/c7nj03113k
28. Adeleke A, Zamisa SJ, Omondi B. Crystal structure of dichlorido-bis((E)-2-((pyridin-4-ylmethylene)amino)phenol)zinc(II), $C_{24}H_{20}Cl_2N_4O_2Zn$. Z Kristallogr NCS. 2020;235(3):625-628. https://doi.org/10.1515/ncrs-2019-0863
29. Adeleke A, Zamisa SJ, Omondi B. Ag(I) complexes of imine derivatives of unexpected 2-thiophenemethylamine homo-coupling and bis-(E)-N-(furan-2-ylmethyl)-1-(quinolin-2-yl)methanimine. Molbank. 2021;2021(2):1-9. https://doi.org/10.3390/m1235
30. SAINT BVA. Data reduction software. Bruker AXS Inc, Madison, Wisconsin, USA. 2009.
31. Bruker A. Saint and sadabs. Bruker AXS Inc, Madison, Wisconsin, USA. 2009.
32. Sheldrick G. Crystal structure solution with SHELXT. Acta Crystallogr A. 2015;71:3-8. https://doi.org/10.1107/S2053273314026370
33. Farrugia L. WinGX and ORTEP for Windows: An update. J Appl Cryst. 2012;45(4):849-854. https://doi.org/10.1107/S0021889812029111
34. Sheldrick G. Crystal structure refinement with SHELXL. Acta Crystallogr C Struct Chem. 2015;71(Pt 1):3-8. https://doi.org/10.1107/S2053229614024218
35. Njogu E, Omondi B, Nyamori VO. Silver(I)-pyridinyl Schiff base complexes: Synthesis, characterisation and antimicrobial studies. J Mol Struct. 2017;1135:118-128. https://doi.org/10.1016/j.molstruc.2017.01.061

36. Adeleke AA, Zamisa SJ, Islam MdS, Olofinsan K, Salau VF, Mocktar C, Omondi B. A study of structure-activity relationship and anion-controlled quinolinyl Ag(I) complexes as antimicrobial and antioxidant agents as well as their interaction with macromolecules. Biometals. 2022;35(2):363-394. https://doi.org/10.1007/s10534-022-00377-6
37. Benzie I, Strain JJ. The ferric reducing ability of plasma (frap) as a measure of "antioxidant power": The frap assay. Anal Biochem. 1996;239(1):70-76. https://doi.org/10.1006/abio.1996.0292
38. Adeleke A, Zamisa SJ, Islam MdS, Olofinsan K, Salau VF, Mocktar C, Omondi B. Quinoline functionalized schiff base silver(I) complexes: Interactions with biomolecules and in vitro cytotoxicity, antioxidant and antimicrobial activities. Molecules. 2021;26(5):1205. https://www.mdpi.com/1420-3049/26/5/1205
39. Abrahams S, Mosebi S, Fish MQ, Papathanasopoulos MA, Hewer R. Screening of the nih clinical collection for inhibitors of hiv-1 integrase activity. S Afr J Chem. 2018;114(3-4):1-5. https://doi.org/10.17159/SAJS.2018%2F20170324
40. Rendosova M, Vargova Z, Kuchar J, Sabolova D, Levoca S, Kudlacova J, Paulikova H, Hudecova D, Helebrandtova V, Almasi M, Vilkova M, Dusek M, Bobalova D. New silver complexes with bioactive glycine and nicotinamide molecules - characterization, DNA binding, antimicrobial and anticancer evaluation. J Inorg Biochem. 2017;168:1-12. https://doi.org/10.1016/j.jinorgbio.2016.12.003
41. Patel M, Parmar PA, Gandhi DS. Synthesis, characterization and DNA binding and cleavage properties of ruthenium(II) complexes with various polypyridyls. J Enzyme Inhib Med Chem. 2011;26(5):734-741. https://doi.org/10.3109/14756366.2011.570007
42. Gomathi A, Vijayan P, Viswanathamurthi P, Suresh S, Nandhakumar R, Hashimoto T. Organoruthenium(II) compounds with pyridyl benzoxazole/benzthiazole moiety: Studies on DNA/protein binding and enzyme mimetic activities. J Coord Chem. 2017;70(10):1645-1666. https://doi.org/10.1080/00958972.2017.1309649
43. Anjomshoa M, Fatemi SJ, Torkzadeh-Mahani M, Hadadzadeh H. DNA- and BSA-binding studies and anticancer activity against human breast cancer cells (mcf-7) of the zinc(II) complex coordinated by 5,6-diphenyl-3-(2-pyridyl)-1,2,4-triazine. Spectrochim Acta A Mol Biomol Spectrosc. 2014;127:511-520. https://doi.org/10.1016/j.saa.2014.02.048
44. Adeleke AA, Islam MS, Omondi B. Silver(I) pyridinyl complexes with benzothiazole, thiophene, and furan moieties: DNA/protein-binding, antibacterial, antioxidant, and anticancer studies. Arch Pharm (Weinheim). 2023;356:e2200308. https://doi.org/10.1002/ardp.202200308
45. Hong M, Geng H, Niu M, Wang F, Li D, Liu J, Yin H. Organotin(IV) complexes derived from schiff base N'-[(1E)-(2-hydroxy-3-methoxyphenyl) methylidene]pyridine-4-carbohydrazone: Synthesis, in vitro cytotoxicities and DNA/bsa interaction. Eur J Med Chem. 2014;86:550-561. https://doi.org/10.1016/j.ejmech.2014.08.070
46. Kong L, Yu H, Zhang J, Cui W. Tetra-aqua-bis-[N,N'-bis-(pyridin-3-yl-methyl-idene)benzene-1,4-diamine]-zinc dinitrate 1.49-hydrate. Acta Crystallogr Sect E Struct Rep Online. 2011;67(Pt 12):m1752. https://doi.org/10.1107/S1600536811046915
47. Lamming G, Kolokotroni J, Harrison T, Penfold TJ, Clegg W, Waddell PG, Probert MR, Houlton A. Structural diversity and argentophilic interactions in one-dimensional silver-based coordination polymers. Crystal Growth & Design. 2017;17(11):5753-5763. https://doi.org/10.1021/acs.cgd.7b00752
48. Wu H-C, Thanasekaran P, Tsai C-H, Wu J-Y, Huang S-M, Wen Y-S, Lu K-L. Self-assembly, reorganization, and photophysical properties of silver(I)–schiff-base molecular rectangle and polymeric array species. Inorg Chem. 2006;45(1):295–303. https://doi.org/10.1021/ic051235k
49. Pucci D, Barberio G, Bellusci A, Crispini A, La Deda M, Ghedini M, Szerb EI. Induction of columnar mesomorphism in tetracoordinated ionic silver(I) complexes based on chelate 4,4'-disubstituted 2,2'-bipyridines. Eur J Inorg Chem. 2005;2005(12):2457-2463. https://doi.org/10.1002/ejic.200500002
50. Li H, Liu C, Dai B, Tang X, Zhang ZJ, Xiong Z, Liu X. Synthesis, conductivity, and electromagnetic wave absorption properties of chiral poly schiff bases and their silver complexes. J Appl Polym Sci. 2015;132(36):1-8. https://doi.org/10.1002/app.42498
51. Njogu E, Omondi B, Nyamori VO. Coordination polymers and discrete complexes of Ag(I)-n-(pyridylmethylene)anilines: Synthesis, crystal structures and photophysical properties. J Coord Chem. 2017;70(16):2796-2814. https://doi.org/10.1080/00958972.2017.1370088
52. Russell AD. Types of antibiotics and synthetic antimicrobial agents. Hugo and Russell's Pharmaceutical Microbiology. 2004:152-186. https://doi.org/10.1002/9780470988329.ch10
53. Nandhini P, Kumar P, Mickymaray S, Alothaim AS, Somasundaram J, Rajan M. Recent developments in methicillin-resistant staphylococcus aureus (MRSA) treatment: A review. Antibiotics (Basel). 2022;11(5). https://doi.org/10.3390/antibiotics11050606
54. Guentzel M. Chapter 26, escherichia, klebsiella, enterobacter, serratia, citrobacter, and proteus. Medical Microbiology, 4th Edn, ed S Baron (Galveston: University of Texas, Medical Branch) Available online at: http://wwwncbinlmnihgov/books/NBK8035/ 1996.
55. Patel C, Bassin JP, Scott M, Flye J, Hunter AP, Martin L, Goyal M. Synthesis and antimicrobial activity of 1,2-benzothiazine derivatives. Molecules. 2016;21(7):1-16. https://doi.org/10.3390/molecules21070861
56. Matos M, Vazquez-Rodriguez S, Santana L, Uriarte E, Fuentes-Edfuf C, Santos Y, Munoz-Crego A. Synthesis and structure-activity relationships of novel amino/nitro substituted 3-arylcoumarins as antibacterial agents. Molecules. 2013;18(2):1394-1404. https://doi.org/10.3390/molecules18021394
57. Pasdar H, Hedayati Saghavaz B, Foroughifar N, Davallo M. Synthesis, characterization and antibacterial activity of novel 1,3-diethyl-1,3-bis(4-nitrophenyl)urea and its metal(II) complexes. Molecules. 2017;22(12):1-12. https://doi.org/10.3390/molecules22122125
58. Gök Y, Sarı Y, Akkoç S, Özdemir İ, Günal S. Antimicrobial studies of n-heterocyclic carbene silver complexes containing benzimidazol-2-ylidene ligand. Int J Inorg Chem. 2014;2014:1-6. https://doi.org/10.1155/2014/191054
59. Jimenez J, Chakraborty I, Rojas-Andrade M, Mascharak PK. Silver complexes of ligands derived from adamantylamines: Water-soluble silver-donating compounds with antibacterial properties. J Inorg Biochem. 2017;168:13-17. https://doi.org/10.1016/j.jinorgbio.2016.12.009
60. Cifuentes-Vaca O, Andrades-Lagos J, Campanini-Salinas J, Laguna A, Vásquez-Velásquez D, Concepción Gimeno M. Silver(I) and copper(I) complexes with a schiff base derived from 2-aminofluorene with promising antibacterial activity. Inorg Chim Acta. 2019;489:275-279. https://doi.org/10.1016/j.ica.2019.02.033
61. Giacomelli C, Miranda FdaS, Goncalves NS, Spinelli A. Antioxidant activity of phenolic and related compounds: A density functional theory study on the o-h bond dissociation enthalpy. Redox Rep. 2004;9(5):263-269. https://doi.org/10.1179/135100004225006038
62. Irshad M, Zafaryab M, Singh M, Rizvi MM. Comparative analysis of the antioxidant activity of cassia fistula extracts. Int J Med Chem. 2012;2012:157125. https://doi.org/10.1155/2012/157125
63. Adeleke AA, Islam MdS, Olofinsan K, Salau VF, Mocktar C, Omondi B. Evaluation of substituent bioactivity and anion impact of linear and t-shaped silver(I) pyridinyl complexes as potential antiproliferative, antioxidant, antimicrobial agents and DNA- and bsa-binders. New J Chem. 2021;45(38):17827-17846. https://doi.org/10.1039/d1nj03231c
64. El Jemli M, Kamal R, Marmouzi I, Zerrouki A, Cherrah Y, Alaoui K. Radical-scavenging activity and ferric reducing ability of juniperus thurifera (L.), J. Oxycedrus (L.), J. Phoenicea (L.) and tetraclinis articulata (L.). Adv Pharmacol Sci. 2016;2016:6392656. https://doi.org/10.1155/2016/6392656
65. Sreelatha T, Kandhasamy S, Dinesh R, Shruthy S, Shweta S, Mukesh D, Karunagaran D, Balaji R, Mathivanan N, Perumal PT. Synthesis and sar study of novel anticancer and antimicrobial naphthoquinone amide derivatives. Bioorg Med Chem Lett. 2014;24(15):3647-3651. https://doi.org/10.1016/j.bmcl.2014.04.080
66. Duric S, Vojnovic S, Andrejevic TP, Stevanovic NL, Savic ND, Nikodinovic-Runic J, Glisic BD, Djuran MI. Antimicrobial activity and DNA/bsa binding affinity of polynuclear silver(I) complexes with 1,2-bis(4-pyridyl)ethane/ethene as bridging ligands. Bioinorg Chem Appl. 2020;2020(3812050):1-12. https://doi.org/10.1155/2020/3812050
67. Banti C, Giannoulis AD, Kourkoumelis N, Owczarzak AM, Poyraz M, Kubicki M, Charalabopoulos K, Hadjikakou SK. Mixed ligand-silver(I) complexes with anti-inflammatory agents which can bind to lipoxygenase and calf-thymus DNA, modulating their function and inducing apoptosis. Metallomics. 2012;4(6):545-560. https://doi.org/10.1039/c2mt20039b
68. Kazemi Z, Rudbari HA, Mirkhani V, Sahihi M, Moghadam M,

Tangestaninejad S, Mohammadpoor-Baltork I. Synthesis, characterization, crystal structure, DNA- and hsa-binding studies of a dinuclear schiff base Zn(II) complex derived from 2-hydroxynaphtaldehyde and 2-picolylamine. J Mol Struct. 2015;1096:110-120. https://doi.org/10.1016/j.molstruc.2015.04.033

69. Saeidifar M, Jam ZS, Shahraki S, Khanlarkhani A, Javaheri M, Divsalar A, Mansouri-Torshizi H, Akbar Saboury A. Multi-spectroscopic and electrochemical approaches of the interaction between a new binuclear agent and DNA. J Biomol Struct Dyn. 2017;35(12):2557-2564. https://doi.org/10.1080/07391102.2016.1229635
70. Topala T, Bodoki A, Oprean L, Oprean R. Bovine serum albumin interactions with metal complexes. Clujul Med. 2014;87(4):215-219. https://doi.org/10.15386/cjmed-357
71. Lakowicz J. 1983. Protein fluorescence. Principles of fluorescence spectroscopy. Springer. p. 341-381.
72. Adeleke AA, Islam MdS, Sanni O, Mocktar C, Zamisa SJ, Omondi B. Aryl variation and anion effect on ct-DNA binding and in vitro biological studies of pyridinyl Ag(I) complexes. J Inorg Biochem. 2021;214:1-17. https://doi.org/10.1016/j.jinorgbio.2020.111266
73. Prashanth M, Madaiah M, Revanasiddappa HD, Amruthesh KN. Synthesis, characterization, and bsa binding studies of some new benzamides related to schiff base. ISRN Org Chem. 2013;2013:791591. https://doi.org/10.1155/2013/791591